University of California
Los Angeles

Thermomechanical Design of Deformable Laser Mirrors for High Power Applications

A thesis submitted in partial satisfaction
of the requirements for the degree
Master of Science in Mechanical Engineering

by

Razvan Ungureanu

2004

The thesis of Razvan Ungureanu is approved.

V. Gupta

Thomas Hahn

Nasr M. Ghoniem, Committee Chair

University of California, Los Angeles

2004

To my beloved mother.

Table of Contents

List of Figures

List of Tables

Acknowledgments

I want to thank Professor Nasr M. Ghoniem for his valuable guidance and support, Dr. Shahram Sharafat for his quick response when help was needed and all members of the MS 2000 lab.

Abstract of the Thesis

Thermomechanical Design of Deformable Laser Mirrors for High Power Applications

by

Razvan Ungureanu

Master of Science in Mechanical Engineering

University of California, Los Angeles, 2004

Professor Nasr M. Ghoniem, Chair

The aim of the following research and design work was to develop a model for deformable segmented mirrors which can handle high power laser applications. The design work began with the 3D modelling of a mirror assembly that complies with the requirements of the National Ignition Facility for the Inertial Confinement Fusion process. After the completion of the model, several aspects of the structure such as thermo-mechanical and optical response were investigated. The above mentioned process was facilitated by the use of finite element analysis software such as ANSYS and COSMOS Works. The results were then compared to theoretical prediction methods such as Dr. James P. Blanchard's solution for thermal stress due to surface heating. Finally the optical reliability and precision of the system were verified. The results of the analysis show that the mirror assembly is structurally sound, being able to handle a wide range of thermal pulses with virtually no damage. The structure is also able to respect the optical requirements within functional limits. These qualities of the UCLA design for deformable laser mirrors show that it is a promising candidate for the reflection and focusing segment of the Inertial Confinement Fusion project.

CHAPTER 1

Introduction and Thesis Objectives

1.1 Brief Overview of Fusion Processes

In the last few decades cost efficient production of energy has been a constantly researched subject, due in part to the continuing decrease in energy resources in the world. A considerable amount of work has been invested in fusion and fission. Fusion is one of the energy producing methods that have been strongly investigated. The advantage of this process is that fuel can be readily found and it is relatively low cost. Fusion is also a non polluting process which makes it easy to implement at different locations. The most suitable fuel for fusion processes is a combination of two heavy isotopes of Hydrogen - Deuterium and Tritium. There are currently two types of fusion reactors being used - Magnetic Confinement and Inertial Confinement. Magnetic Confinement reactors were the first ones to be constructed and tested. Within these enclosures, magnetic fields are used to contain the charged particles that compose the hot plasma and keep it away from the chamber walls. This method is used for containing the plasma for a relatively long time at a low density. Magnetic Confinement rests upon the property that charged particles, like those in a plasma, will travel along the lines of a magnetic field. By arranging magnetic fields in just the right way, scientists have been able to "trap" the plasma within the fields. While the plasma is held, it can be heated through a combination of microwaves, particle beams, and

the heating generated from currents flowing through the plasma. The plasma density in a magnetically confined reactor is roughly 1015 particles/cm3, which is thousands of times less dense than that of air at room temperature. One of the more recently used magnetic reactors is the Tokomak. It it a closed structure of toroidal shape which uses large coils wrapped around its circumference to induce a powerful magnetic field. Fusion takes place here due to very high compression provided by the magnetic field.

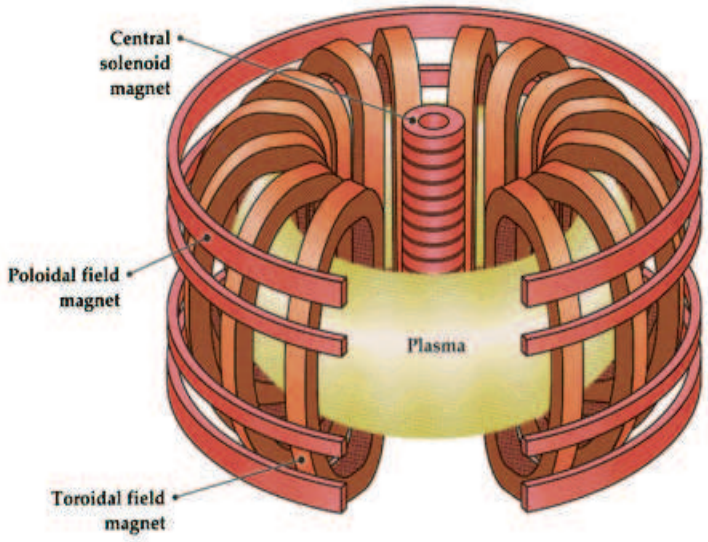

Figure 1.1: Tokomak Fusion reactor

In this type of reactor fusion is a continuous process. In contrast, Inertial Confinement Fusion is a pulsed process. In this process, highly concentrated Deuterium and Tritium pellets are compressed by a large energy load delivered via High Power Lasers. The pellets implode and during this process give off a large amount of thermal energy, Xrays, protons and Helium gas and other particles. The thermal energy is harvested by a wall blanket system and then transported further on to an electrical energy converter. Of course, this process needs to be

contained and there are a few alternatives available for the containment chamber architecture. An ongoing project is currently building such a reactor chamber at the National Ignition Facility located at the Lawrence Livermoore National Laboratory[**?**].

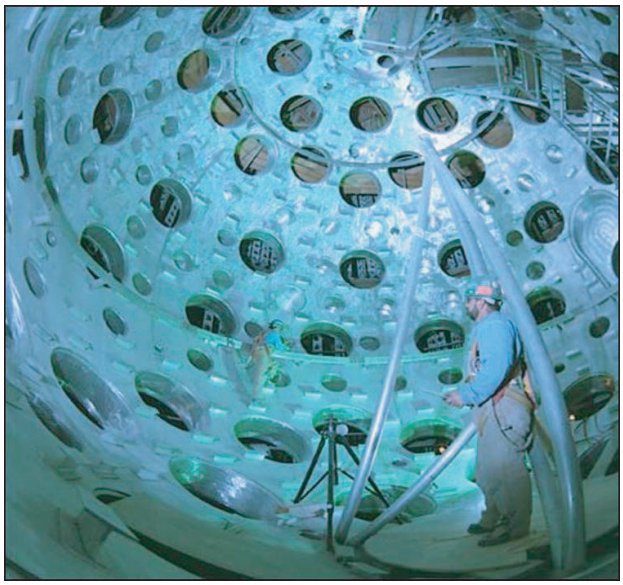

Figure 1.2: Fusion Reactor(Lawrence Livermoore National Laboratory)

There are currently two approaches to compress the Deuterium Tritium pellets: direct-drive laser fusion and indirect-drive laser fusion[**?**]. In the direct-drive method, many intense laser beams are focused symmetrically on a hollow plastic pellet filled with a mixture of deuterium and tritium gas. The intense focused energy ablates the shell, and the subsequent rocket action implodes the inner part of the shell, compressing the gas. Substantial nuclear energy gain results if the compressed gas reaches densities of the order of 1000 times that of liquid DT, along with sufficient heating of the gas. In the indirect approach, a pellet is centered within an enclosure (called a "hohlraum"). A few intense laser beams entering the enclosure and striking the walls create x rays. The subse-

quent "cloud" of x rays then symmetrically ablates the pellet shell and produces the required compression and heating.

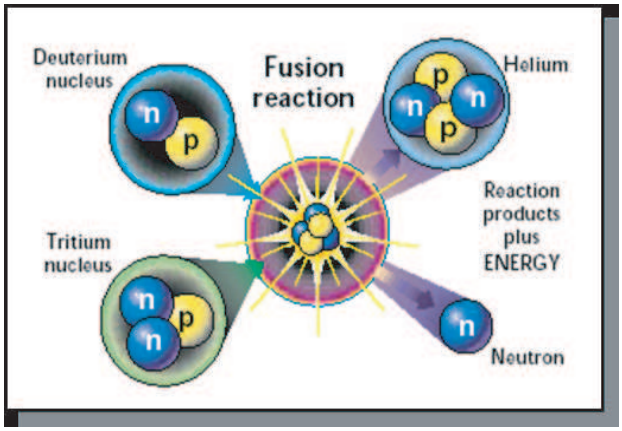

Figure 1.3: Inertial Fusion Raction

Although the work presented here is based around the direct drive method, the design can easily be applied to the indirect method if certain changes are implemented. There are also a few military applications that would benefit form the development of such a system. Although it is still in the research and development stage, Inertial Confinement Fusion is a promising concept.

1.2 Role and Significance of Opto-Mechanical System

The Inertial Fusion Process requires a complex system. Besides the confinement chamber the laser delivery system is also crucial to the process execution. The laser sources provide a pulsed load of 10 watts per square centimeter average power . The laser beams will then follow a path dictated by the Optical System and will ultimately focus onto the target inside the reactor chamber. Therefore the Opto- Mechanical System is required to handle a large energy load and be able to manipulate the laser beams along their path to the target. As outlined be-

fore, two specific tasks are required of the Optical System of the Inertial Fusion Project; reflection of the laser rays and focusing onto the target. It is important to keep in mind that the error involved in this process has to be minimal. In case of misfiring, the fuel could ignite non-symmetrically and produce a deformed explosion. This type of response could in turn damage the containment chamber. Multiple methods of handling the laser load have been researched. The National Ignition Facility is currently using a system of flat surface mirrors and KDP crystals[?] to control the Opto-Mechanical System. Within this approach,reflection is achieved by flat mirrors and focusing is facilitated by a series of prisms and crystals.

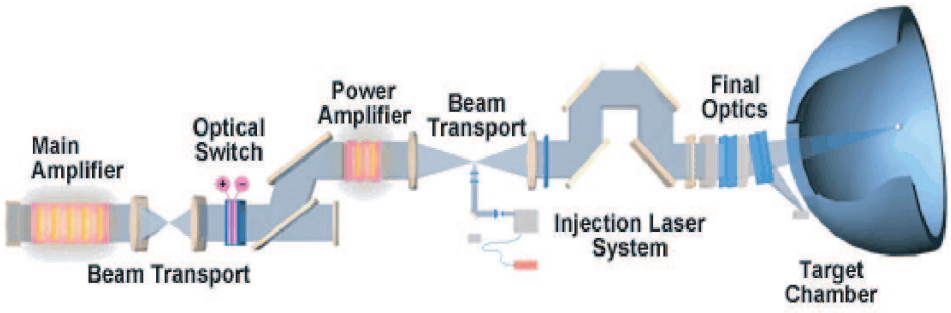

Figure 1.4: NIF optical path

The actual final optics used in this system are a set of KDP crystals grown specifically for focusing purposes of the laser beams. Although the precision level of these optical components is expected to be satisfactory, there are few factors that make them unsuitable for mass production. These crystals are rather large and expensive to manufacture. The manufacturing process is also rather complicated and timely. They have to be very precise since the target is a pellet of a few millimeters. The design for the final optics of the Inertial Fusion Process outlined in this document provides an alternate solution to the crystal prism

focusing method. The UCLA Grazing Mirror Design performs all the required tasks necessary to achieve the purpose of the final optics. It achieves focusing and reflection in a controlled manner thus ensuring the proper outcome for the fusion process. Below, the entire focusing structure is shown.

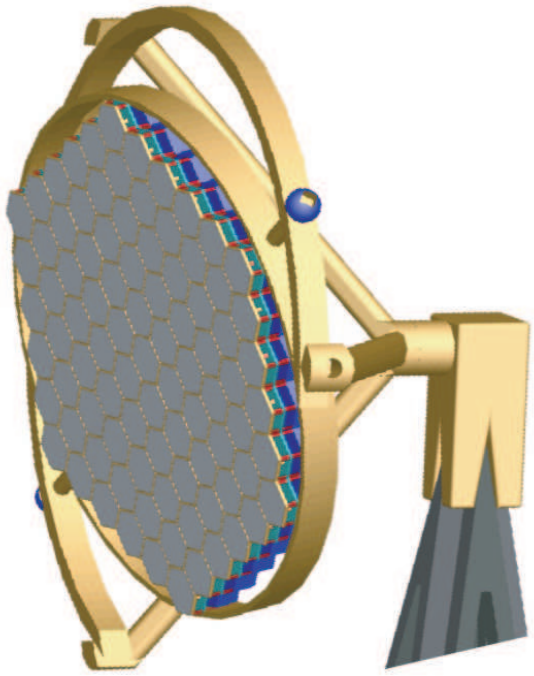

Figure 1.5: UCLA Design of Final Optics

Detailed description of every component involved in this assembly will be provided in the thesis. As expressed before, this work will show how all the involved subsystems of the UCLA design work together to provide the necessary features for a feasible option of the final optics of the Inertial Fusion Process.

1.3 Thesis Objectives

The overall objectives of this thesis can be stated as follows:

- Design a feasible final focusing option for the Inertial Fusion Process.
- Provide a system that is able to reflect the High Average Power Lasers and at the same time be able to focus the rays onto the target. A control system is also associated with the focusing section. Focusing is a highly important function of the system that will be described in detail.
- Demonstrate the thermo-mechanical capabilities of the UCLA Grazing Mirror Design. Detailed thermal and mechanical analysis is presented throughout the thesis.
- Offer a reliable and economical solution to using KDP crystals as the final optics system for the Inertial Fusion Project.

Inertial Fusion has been a highly researched subject in the last few years. The major interest in this subject is due to the opportunity of offering an alternative solution to energy production that is relatively low cost and has a high safety rating[**?**]. The UCLA Grazing Mirror Design plays an important role in the development of reliable, long term use optics for the fusion process. Its features ensure reliability, precision and longevity in the inertial fusion world. Designed as an alternative solution to the NIF KDP crystals final optics system, the UCLA Grazing Mirror brings to the table many qualities such as versatility and lower operating costs. Its ability to reflect and focus the laser beams provides a good replacement for other systems that require many components to achieve the same final result. It also features a control system that allows the mirror to change its surface as required by the position of the target. It is able not only to deform

its surface but also to compensate for any potential damage to the surface of the mirror by slightly tilting its smaller components. Along with its deformable surface, the UCLA Design is able to completely reorient the entire structure to a prescribed position. The work outlined here will show through analysis that the UCLA Design is able to withstand the thermal loads applied by the laser beams without any major damage to its surface. The results are also checked against previous results obtained for surface heating of Aluminum structures. This comparison shows and further strengthens the correctness of the analysis conducted. Further details are then provided about the control system required for deformable optics and an evaluation of the precision of this system is then offered.

CHAPTER 2

Previous Research and Types of Deformable Mirrors

Deformable mirrors are an interesting subject of research in today's advanced world of optics. Such mirrors are used in a multitude of areas ranging from space applications to lasers. This chapter provides a list of previous research works on deformable mirrors and their impact on today's advancements. A few different types of deformable mirrors are described and their advantages are provided. The focus of this section is based on a description of large surface area mirrors, since considerable size is required by the Inertial Fusion Process parameters. The categorization of these mirrors is dictated by the surface texture parameter. Three main categories will be covered:

- Segmented Deformable Mirrors. This type is mainly found in Space Telescopes Applications.
- Continuous Face Sheet Deformable Mirrors. These mirrors have also been used in multiple areas such as telescopes and military applications.
- Bimorph Mirrors. This type is a fairly new concept in the large deformable mirror industry. Its applications are gaged towards lasers and satellite solar panels.

The UCLA Grazing Mirror is hybrid design made up of a combination of features found in the mirrors listed above. The large assembly is made up of 91 segments; each segment is in turn deformable. This approach provides the UCLA design with the versatility necessary to achieve the required tasks.

2.1 Segmented Deformable Mirrors

Early segmented mirrors were mainly composed of a few small partitions, each controlled by three actuators. For an initial design, this concept is feasible, but as we will see the surface profile of the segments can not be changed. This feature renders this type of design unusable for high laser power applications since its surface is not able to compensate for surface swelling nor does it provide a focusing feature at the segment level. Although High Average Power Lasers might be difficult to handle with such a design, there are quite a few areas where these mirrors excel. Such an example would be NAOMI which is part of the William Herskel Telescope in the UK. Below is a diagram of a typical Segmented Mirror profile[**?**].

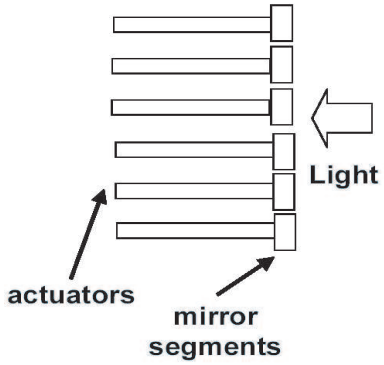

Figure 2.1: Segmented deformable Mirror Profile

The choice of actuators and materials for the surface of the mirror are obviously determining factors in the reliability of this type of mirrors. As mentioned above NAOMI is a good example of a Segmented Deformable Mirror. Shown below is a front view of the actual mirror[**?**].

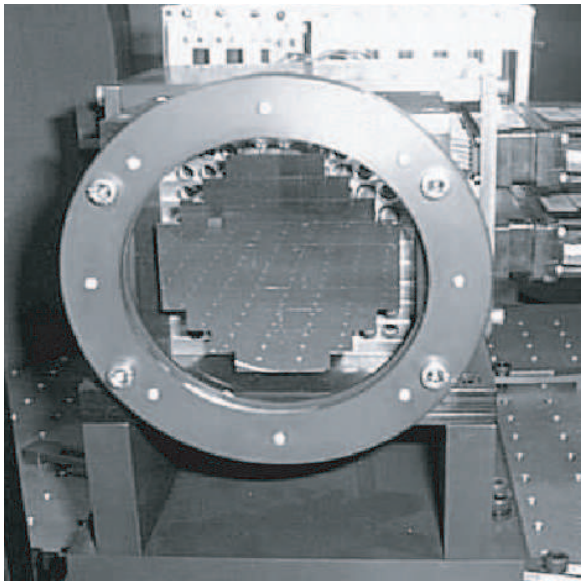

Figure 2.2: NAOMI British Telescope Mirror

This mirror is made up of a multitude of square segments. These segments are controlled by three piezoelectric actuators, each of which has a strain gage attached to it. Strain gauges provide independent measure of movement thus providing the possibility of a control system for the mirror.They are also used to reduce hysteresis to below 1 percent. This in itself is a great achievement since piezoelectric actuators usually have up to 10 percent hysteresis. The largest segmented mirror produced was fabricated in the early 90's. Named Thermotrex, this mirror was primarily designed for military purposes. It features 512 segments each of which is controlled by three push and pull piezoelectric actuators. Its overall diameter stands at 22 cm wide.

2.2 Continuous Face Sheet Deformable Mirrors

As outlined before, early deformable mirrors (DMs) consisted of discreet segments, each controlled by 3 piezoelectric actuators. Nowadays, a common technology is to bond a thin faceplate to an array of piezoelectric actuators (see the Figure). The actuators are not produced individually, but rather a multi-layer wafer of piezo-ceramic is separated into individual actuators. This type of DMs is used in the GEMINI AO systems.

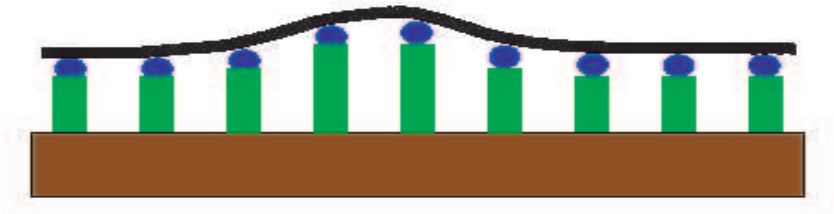

Figure 2.3: Continuous Face Sheet Profile

Certain characteristics of the Continuous Face Sheet Mirrors have to be satisfied in order to obtain optimal functionality[**?**]:

- Facesheet thickness must be large enough to maintain flatness during polishing, but low enough to deflect when pushed or pulled by actuators .
- Thickness also has to be adequate for the "influence function" which is defined as the response of mirror shape to push by one actuator.
- Actuators also have to be stiff as well, so they won't bend sideways as the mirror deflects.

The table below emphasizes some typical parameters of continuous Face Sheet Mirrors[**?**].

Table 2.1: Properties of Continuous Face Sheet Mirrors

Parameters, Value	
Number of actuators	100-1500
Inter actuator spacing	2-10 mm
Electrode geometry	rectangular or hexagonal
Voltage	few hundred V
Stroke	few microns
Resonant frequency	few kHz
Cost	very high

An example of a Continuous Face Sheet Mirror would be the Xinetics 349 actuator Deformable Mirror used in the Keck Telescope AO system. Some features of this mirror include push and pull magnetic actuators and also a system for measuring the deflection which utilizes an optical interferometer[**?**]. The picture below illustrates the push pull actuator and the control system associated with them to achieve focusing.

Figure 2.4: Rear View of Xinetics Mirror

2.3 Bimorph Deformable Mirrors

A Bimorph mirror consists of two piezoelectric wafers which are bonded together and are oppositely polarized (parallel to their axes). An array of electrodes is deposited between the two wafers. The front and back surfaces are connected to ground. The front surface acts as a mirror.

When a voltage is applied to an electrode, one wafer contracts and the opposite wafer expands, which produces a local bending. The local curvature being proportional to voltage, these DMs are called curvature mirrors[**?**]. A simple diagram of a Bimorph mirror is shown below:

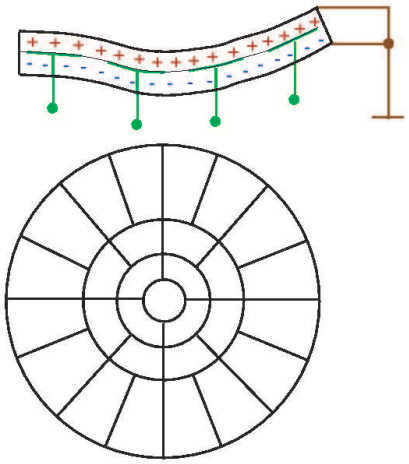

Figure 2.5: Bimorph Mirror Profile

A tricky characteristic of bimorph DMs is that they are controlled not in surface shape, but in surface curvature. For the same applied voltage , the amount of the deformation produced is proportional to , where is the spatial size of the deformed region. Similarly, the saturation of the piezoelectric ceramic must be specified not in terms of surface stroke, but in terms of maximum curvature.

The geometry of electrodes in bimorph DMs is radial-circular, to match best the circular telescope apertures with central obscuration. In this way, for a given number of electrodes (i.e. a given number of controlled parameters) bimorph DMs reach the highest degree of turbulence compensation, better than segmented DMs.

There is no such simple thing as influence functions for bimorph DMs. The surface shape as a function of applied voltages must be found from a solution of the Poisson equation which describes deformation of a thin plate under a force applied to it. The boundary conditions must be specified as well to solve this equation[**?**]. In fact, these DMs are made larger than the beam size, and an outer ring of electrodes is used to define the boundary conditions - slopes at the beam periphery.

2.4 Other Types of Deformable Mirrors

New technologies for deformable mirrors are urgently needed. To correct turbulence at extremely large telescopes (30-100 m in diameter) in the visible, DMs with 10000 - 100000 actuators will be required! One possible way to produce such DMs lies in the silicon technology (so-called MOEMS = Micro-Opto-Electro-Mechanical Systems). These DMs are made by micro-lithography, in a way similar to electronic chips, and small mirror elements are deflected by electrostatic forces. The remaining problems of MOEMS are insufficient stroke and a too small size of elements. Another way to control the phase of light consists in using liquid crystals, like in the displays which have up to million controlled elements. Until recently, liquid crystals were too slow, but now this drawback seems to have been overcome. Still, the phase shifts introduced by liquid crystals remain too small and wavelength-dependent. Although there is more research needed for the de-

velopment of MOEMS significant progress has been made so far. A diagram of such a mirror is offered below.

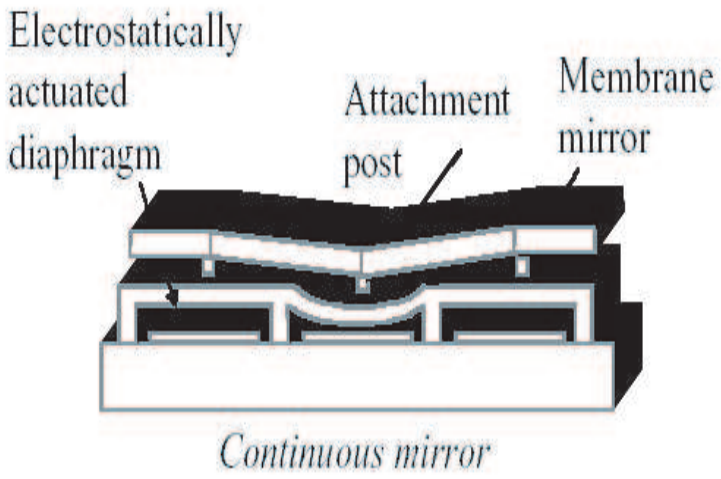

Figure 2.6: MEMS Mirror Profile

CHAPTER 3

High Average Power Laser System Description

The entire Inertial Confinement Fusion system is made up of a series of complex subsystems. From the laser source to the target the laser beams pass through all these subsystems. The initial system is responsible for generating the laser beams for the fusion process. Following is the Intermediary Optics System which guides and filters the laser beams. The next system is the Final Optics System which takes care of the focusing and reflection onto the target pellet. Once in the containment chamber, the laser beams cause the fusion reaction to take place upon compression of the target pellet. From this point on many other subsystems take control of the process and carry it to the end of one full cycle. Figure 3.1 offers an overall view of the entire project design. These facilities are

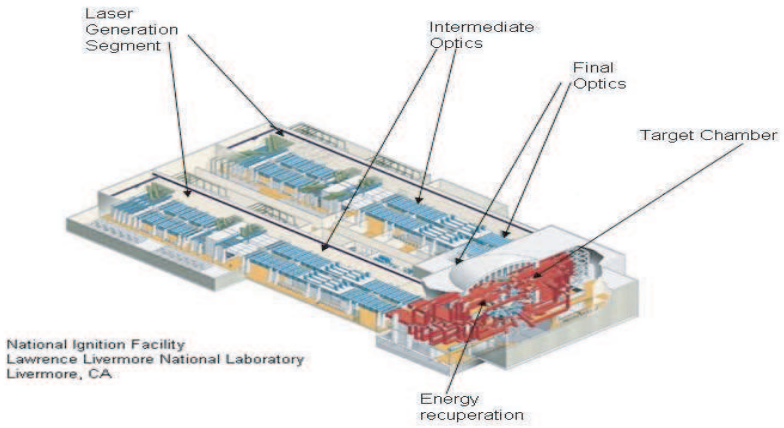

Figure 3.1: NIF Lawrence Livermore Facilities

in their developmental stage at Lawrence Livermore. This section of the thesis contains a rather brief description of the NIF High Average Power Lasers System components and their purpose in the overall fusion process.

3.1 Laser Generation Subsystem

The laser beams are initially generated in the Injection Laser Segment before they enter the main amplifiers. The ILS system uses fiber optics technology and was designed to satisfy the broad range of NIF experimental requirements. Key ILS components include the Master Oscillators and the Preamplifier Modules.

Figure 3.2: NIF Laser Preamplifier

NIF laser pulses are born in the master oscillator room, in which a compact laser oscillator cavity made of ytterbium-doped optical fiber generates low-energy laser pulses. The oscillator pulse is shaped in time and frequency- broadened (using the small range of multiple colors produced in the fiber laser) to help smooth the intensity of the laser beam when in it ultimately focused onto the target. Each of the pulses is then transported on separate fiber optic cables to 48

preamplifier modules for further amplification and beam shaping. The amplifiers use 16 glass slabs per beam (and a capability for 18 slabs per beam if necessary). They are arranged in two amplifier sections; the main amplifier and the power amplifier.

Figure 3.3: Laser Glass Assemblies for the Amplifiers

When coupled together these amplifiers produce 99.9 percent of the required power and energy for the NIF Inertial Fusion Process. The amplification section is also the most expensive section of the NIF project.After being released form the amplifying section the beams will enter the Intermediate Optics Segment.

3.2 Intermediate Optics Subsystem

The Intermediate Optics Section of the fusion process is made up of two major types of components;the spatial filters and the switchyard. Spatial filters contain opto-mechanical components that condition and smooth the laser beams, maintaining their precise characteristics throughout transport to the target chamber. The laser pulses travel through two stages of spatial filters. These will focus

the beams through pinholes to remove high-frequency intensity variations. The cavity spatial filters are 23.5-m long, the transport spatial filters are 60-m long.

Figure 3.4: NIF Spatial Filters

After the filters, the laser beams enter what is known as the Switchyard. The main purpose of the switchyard is to redirect the laser beams to the upper and lower hemisphere of the target chamber.

Figure 3.5: NIF Switchyard

This task is achieved by a series of redirecting mirrors that send the laser beams into the target chamber through the Final Optics Segment. The mirrors receive special coatings and subsequent conditioning that enables them to survive within NIF's high-energy laser environment.

3.3 Final Optics Subsystem

The Final Optics section has as purpose the focusing and reflection of the high-power lasers. This section is currently represented at Lawrence Livermore by a set of KDP crystal prisms. The figure below shows one such KDP crystal prism.

Figure 3.6: ICF Current Final Optics

As mentioned before the intention is to replace the KDP crystals with the UCLA Deformable Mirror due to its more advantageous long term use and lower costs. A schematic of the UCLA Final Optics and the Target Chamber Design is shown below. Please observe that there are multiple Grazing Mirrors that have to accomplish the same task at the same time. The current number used for this

design is 64 mirrors.

Figure 3.7: Inertial Fusion Process System

In order to perform the outlined tasks, specific subsystems were designed to deal with each requirement. All these subsystems of the Final Optics of the Inertial Confinement Process are discussed in the next section.

3.4 Inertial Fusion Chamber

The target chamber is the enclosure where the inertial fusion reaction takes place. Its diameter is about 10 meter and it is mostly made of Aluminum and other alloys. Weighing in at about 1,000,000 pounds the fusion chamber represents the interface in between the final optic and the NIF target. The target chamber provides a vacuum environment for the target fusion. Diagnostic instruments, such as x-ray spectrometers, microscopes, and cameras, are mounted around the equator and at the poles of the target chamber using 120 available diagnostic ports. For high-energy-density and fusion ignition experiments, the target is a

metal cylinder–typically made of gold or lead–about 6 mm in diameter and 10-mm long. The cylinder contains a plastic fusion capsule about 3 mm in diameter. The capsule is frozen to a temperature of a few degrees above absolute zero and

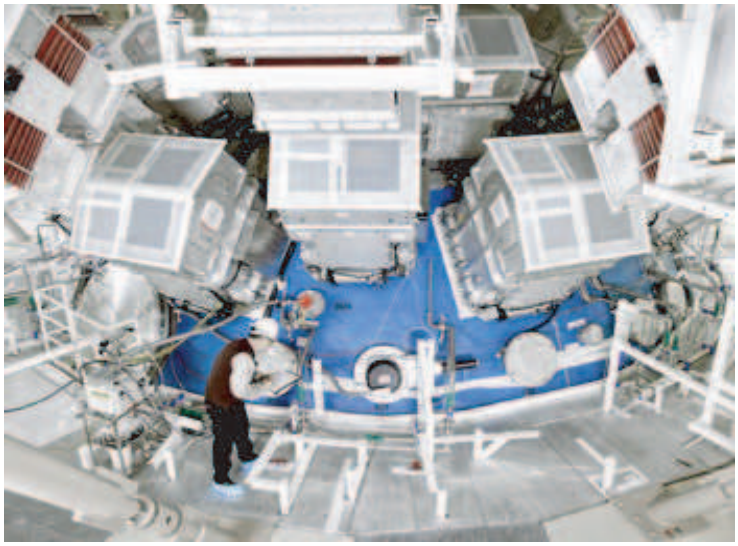

Figure 3.8: Inertial Fusion Chamber

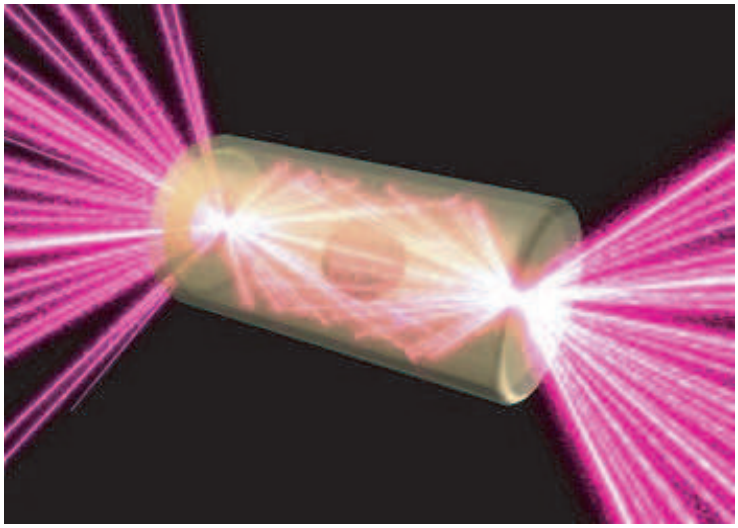

Figure 3.9: Fusion Target

is lined with a layer of solid deuterium-tritium (DT) fusion fuel. The hollow interior contains a small amount of DT gas. Upon ignition the target implodes and releases a tremendous amount of energy into the Fusion Chamber.

CHAPTER 4

UCLA Final Optics Design

The system of interest of this thesis is the Final Optics System. This system is mainly comprised of the optical focusing surface, control system for the surface and a cooling system. In order to perform correctly certain system requirements have to be satisfied:

- Be able to withstand a pulsed average laser load of 10 W per squared cm.
- Correctly reflect and focus a 0.5 meter diameter incident laser beams.
- Be able to correct the surface of the mirror in order to adapt for surface swelling and re-orientation of the target.
- Be structurally sound enough, not to collapse under the induced vibrations.
- Have a high average lifetime under cyclical loading.

4.1 Reflective and Focusing Subsystem

In order to design a surface that is able to reflect and focus a cylindrical beam , a special kind of surface needs to be designed. In the past, concurrent reflection and focusing has been achieved by using an off axis parabolic mirror. The concept is rather elementary, the mirror profile used is the same as the one of a regular parabolic mirror. This profile is commonly found in conventional automotive

lights and high power reflectors. The only difference in this case is that the section of the mirror which will be used to achieve the specified task is taken from an off axis position. By using a segment that does not include the major axis of the parabola, reflection and focusing are guaranteed.

4.1.1 Sub-System Requirements

The system requirements pertaining to the Optical Subsystem are as follows:

- Cover an area of at least 80 cm diameter.
- Have an off axis paraboloid configuration.
- Distance to focal point 14-15 meters.
- Withstand the average power delivered to the surface with no major damage.

In order to achieve all the above requirements, a hybrid mirror with components for both segmented and continuous face mirrors was considered as a candidate.

4.1.2 Background on Off Axis Parabolic Mirrors

The definition of a paraboloidal mirror is as follows[**?**]:

"A concave mirror that has the form of a paraboloid of revolution. The paraboloidal mirror may have only a portion of a paraboloidal surface through which the axis does not pass, and is known as an off-axis paraboloidal mirror. All axial, parallel light rays are focused at the focal point of the paraboloid without spherical aberration, and conversely all light rays emitted from an axial source

at the focal point are reflected as a bundle of parallel rays without spherical aberration."

In this design an off axis paraboloid mirror will be used just as mentioned above.

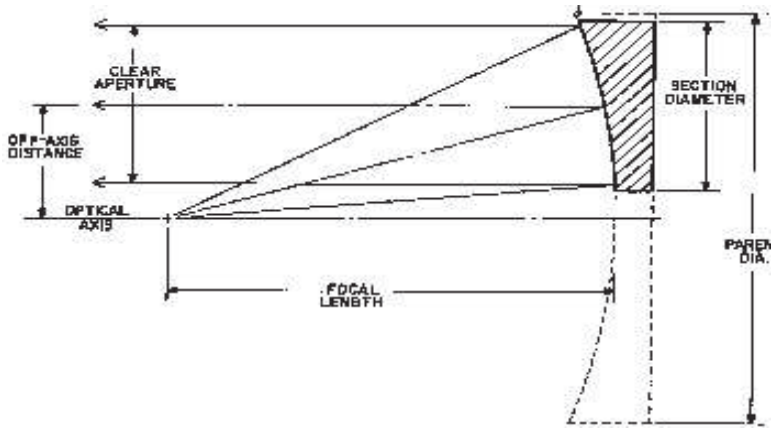

Figure 4.1: Off axis paraboloidal mirror profile

From the basic geometrical description, a paraboloidal mirror has the surface configuration obtained by rotating a parabola around its main axis. The profile of the mirror in 2D is a simple parabola in the XY plane and behaves by the following equation[**?**]:

$$(Y - Y_0)^2 = 4A(X - X_0) \tag{4.1}$$

Where A, also known as the focal length is the distance from the vertex to the diretrix of the parabola. This parameter decides how shallow the parabola will be. In the YZ plane the paraboloid with a certain radius H is described by the equation of a circle:

$$(Y - Y_0)^2 + (Z - Z_0)^2 = H^2 \tag{4.2}$$

4.1.3 Mathematical Surface Formation

This section demonstrates how the exact surface necessary for focusing of the laser beams can be obtained by using a mathematical software package such as Matlab. As expressed before, the portion of the parabolic profile used for the construction of the reflective surface has to be rather shallow in order to insure high reflectivity. The incoming rays will hit the mirror surface at a low incidence angle thus allowing for minimal energy absorption into the final optics segment. Using MATLAB a two dimensional graph can be drawn:

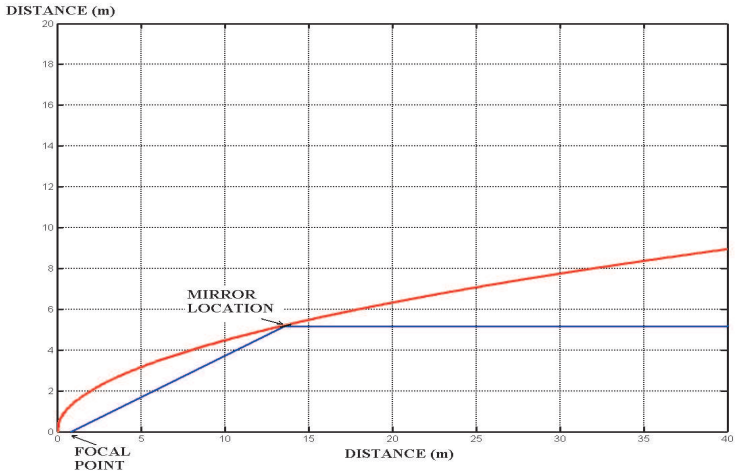

Figure 4.2: 2D Equation Profile

The following parameters have been obeyed when modelling the mirror for proper functionality of the optical system:

- Have a shallow surface configuration to insure low absorption.
- Obeys paraboloid of revolution equation.
- Focal length of the paraboloid has to be around 0.5 meters.

- Distance from center of the mirror of interest to the focal point should be 14 meters.

The resultant 3D surface is that of a paraboloid described by the following equation:

$$(Y - Y_0)^2 + (Z - Z_0)^2 = 2 * X \tag{4.3}$$

The above equation is used to model the following surface. The extracted section shows the approximate portion of the surface used for the unit segment of the mirror.

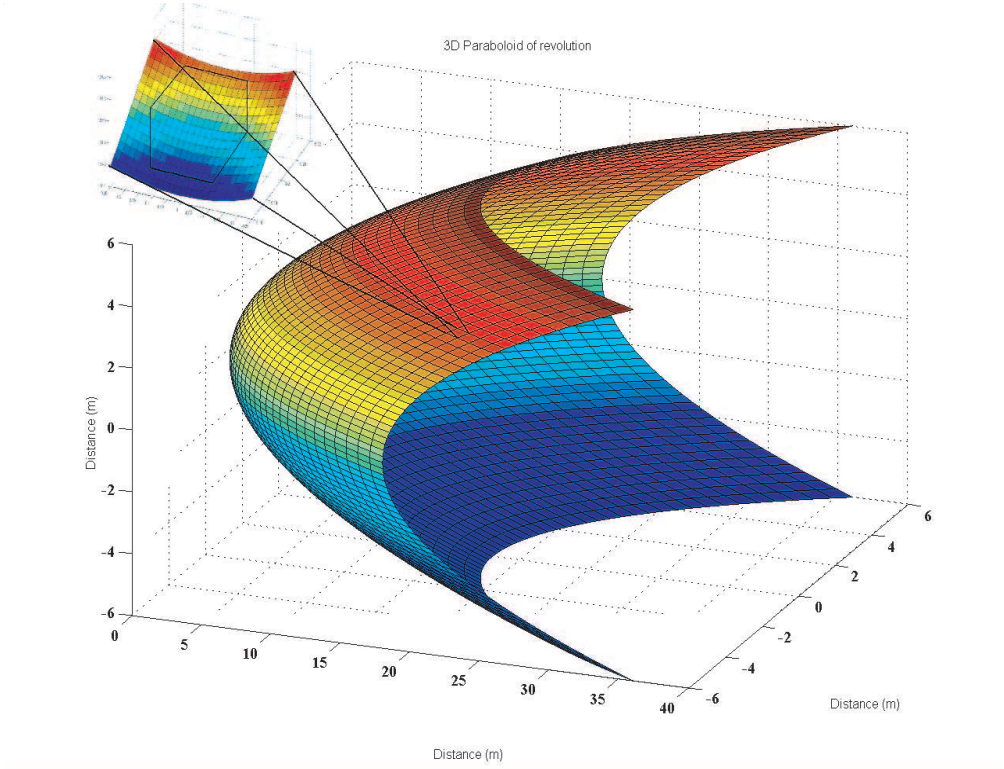

Figure 4.3: 3D Mirror Surface

Using the above mention surface conformation and an incident beam parallel

to the main axis of the parabola, the incidence angle is calculated to 70 degrees. The shallowness of the surface incidence guarantees very low energy absorbance. The points obtained from the surface equation pictured above will be used in the surface control system.

4.1.4 The UCLA Optical Surface Design

Since the surface of the large mirror is segmented, careful attention has to be granted to each and one of the segments. The profile for the segments have been chosen to be hexagonal. This shape has proven to be successful in previous designs since it almost eliminates the possibility of laser leakage between adjacent small mirrors. Modelling of the unit piece segment was achieved using the Solidworks 3D software package. The unit segment,as mentioned before is of hexagonal shape with a radius of 50 millimeters and a thickness of 1 millimeter.

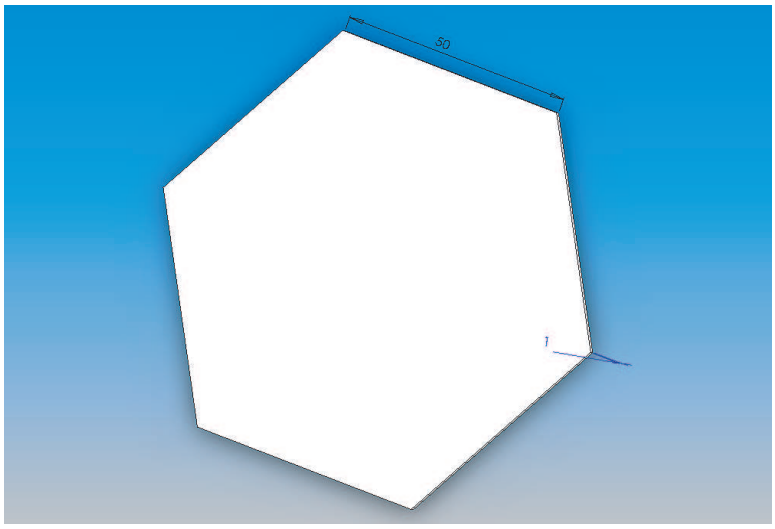

Figure 4.4: Mirror Basic Segment-Solidworks Model

Although the modelled surface is flat it can be deformed to the requirements

imposed by the fusion system. Deformation is achieved through the use of actuators that can push and pull the surface.

4.2 Surface Control Subsystem

The control system design project for the UCLA Conformal Grazing Mirror offers an initial proposal for surface correction and compensation. This system design will show the best combination of parameters that can be used to build the control system for the UCLA Grazing Mirror. Factors such as surface swelling and misalignment are to be compensated for by the control system[**?**]. This is to ensure that the IFC target will be correctly covered. The resulting control system design should be able to focus within 5 percent error of the target surface. There will be an overlapping phenomenon but the benefits of higher accuracy exceed the complications of overlapping. The following illustration is a mere simulation of the target coverage by 12 and 24 incoming laser beams.

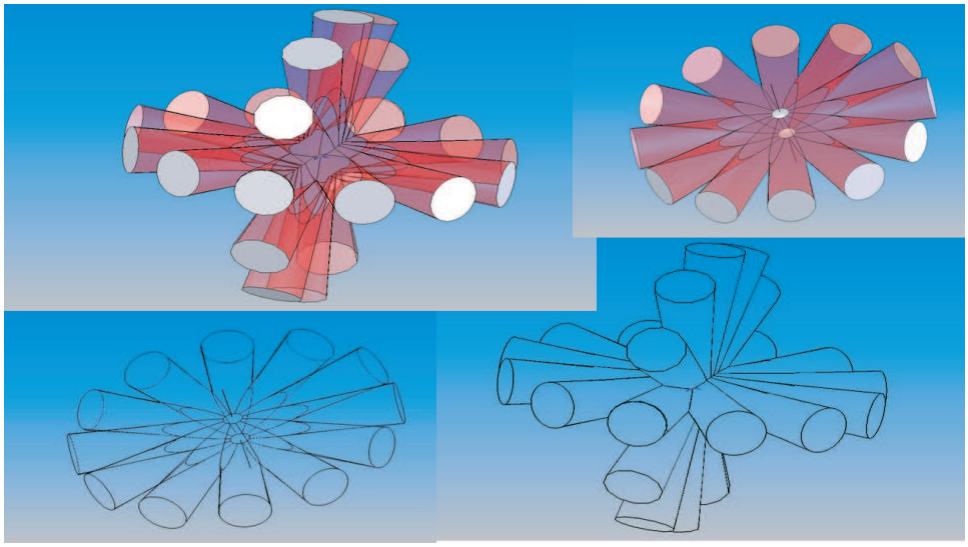

Figure 4.5: NIF Target Coverage

4.2.1 Sub-System Requirements

The requirements for the control system are as follows:

- Low hysteresis deformation of surface.
- Minimal use of actuators for simplicity and cost reduction.
- Ability to pull surface up to 1 millimeter in the vertical direction.
- Symmetrical geometry for actuator position.

In order to satisfy the above mentioned requirements an investigation has been conducted to select the best geometrical configuration and the optimal type of actuators.

4.2.2 Types of Actuators

In order to understand the selection method, a survey of the different available types of actuators has been made. The type of actuators found plausible for the focusing applications was found to be the push and pull actuators, since the surface of the mirror does not require lateral deformation. In this category there are three kinds of actutors available: Piezo-Electric Actuators, Piezo-Magnetic Actuators and Two-Layer Electrode Actuators. Piezo-Electric actuators achieve change in due to the application of a certain voltage. This type of actuators have been previously used in space telescope applications. They are usually made up of a stack of ceramic disks with integrated electrodes. Typically the voltage needed to deform these actuators is 100 to 150 Volts. The hysteresis they will undergo under long term use is approximately 10 percent and temperature variations usually do not influence their precision[**?**]. From an economical viewpoint the Piezo-Electric actuators are rather inexpensive. The cost for a pack of ten rises

to about 250 dollars. The illustration below shows the basic functionality of the PZM actuator. Actuators of this type are placed below the optical surface of

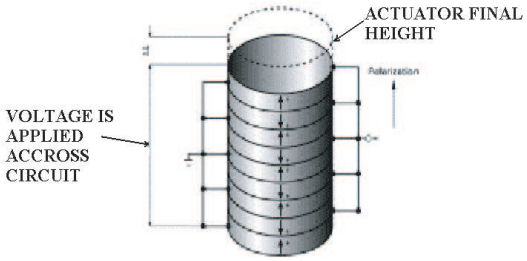

Figure 4.6: PZM actuator

the mirror allowing for movement in the vertical direction. A plot of the voltage applied versus the displacement in the micrometers range of these actuators is shown below.

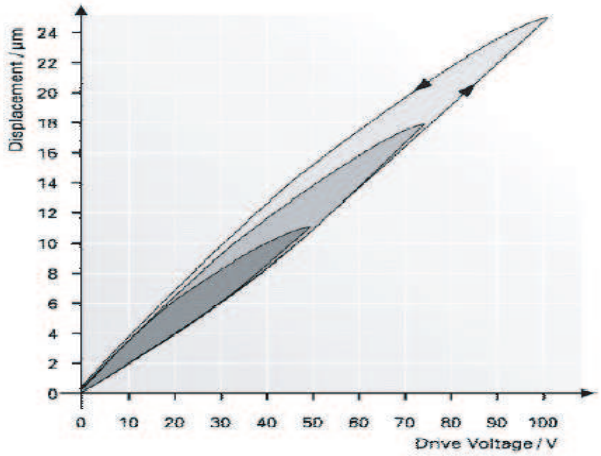

Figure 4.7: PZM actuator hysteresis

The second type of actuator investigated was the Piezo-Magnetic Actuator(PMN). A Piezo- Magnetic actuator changes its length when a magnetic field is applied. The material composition of these actuators is a Lead Magnesium Niobate alloy. These actuators tend to be less expensive than PZM actuators but they are also less precise[**?**].

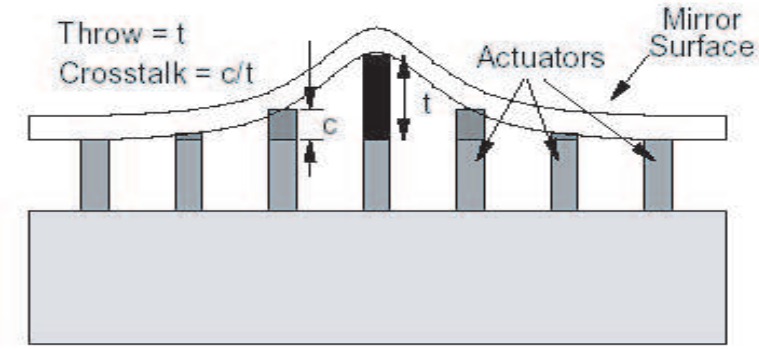

Figure 4.8: Push-Pull Actuators Details

PMN actuators also present a higher hysteresis rate than PMN;about 20 percent. A diagram showing the integration of push and pull actuators (both PZM and PMN)in the mirror system is shown above. The throw T is displacement generated by the actuator in the vertical direction an the crosstalk coefficient is a factor used for determining the influence of one actuator on others. However, if the distance between the actuators is chosen correctly, the crosstalk coefficient can be reduced to almost zero[**?**]. The third type of actuators plausible for the UCLA Deformable Mirror Design is the Two-Layer Electrode Actuators. These actuators are a rather new concept, due to their bold design. As the name says, these actuators use electricity to function and they are separated in two different plates made of dielectric materials. The surface of the two plates presents small protrusions that have symmetric correspondents on the opposite plate. When a

voltage is applied across the electrodes these protrusions move towards or away from each other depending on the direction of the current[?]. Using such a de-

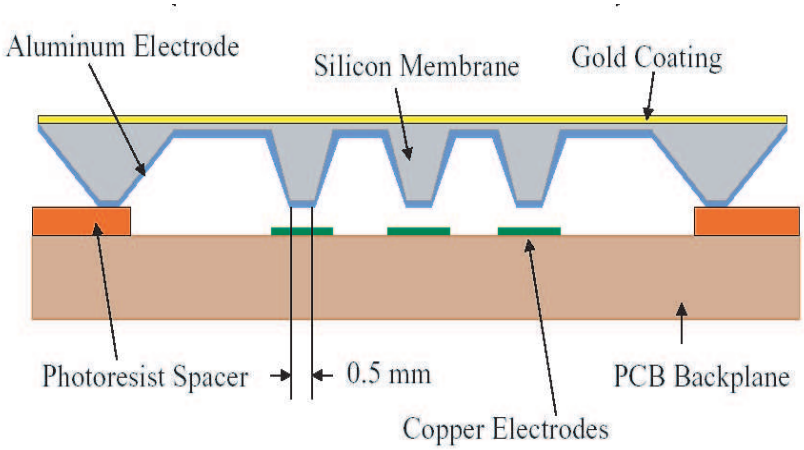

Figure 4.9: Two-Layer Electrode Actuators

sign can increase the precision of the optical surface since the actuator is virtually imbedded in the mirror substrate. The hysteresis associated with these actuators is also quite low; about 5-8 percent providing a feasible solution for the long term use of the optical segment. There is however a larger inter-actuator cross-talk for this kind of actuators. As as seen above, the actuator top layer comes in contact with the reflective surface. This feature can be disadvantageous in case of High Average Power Laser applications. The heat pulse can potentially damage the actuating layer since it is so close to the surface. Since this is a fairly new concept the Two-Layer Electrode actuator can become very expensive.

4.2.3 UCLA Actuator Control System

Using the information provided in the previous section the best candidate for the surface deformation task resulted to be the PZM. The decision is due to the

independence of the ceramic material on temperature fluctuations at the mirror surface. The lower hysteresis coefficient is also a necessary feature for long term applications. The surface to be controlled, as shown in Fig. 4.4 is hexagonal and will be fixed at the corners while the actuators will be placed under the reflective surface in the central area. In order to constrain the mirror surface, a support frame has been designed. This frame will also be used for actuator placement and as infrastructure for the cooling system of the unit piece.

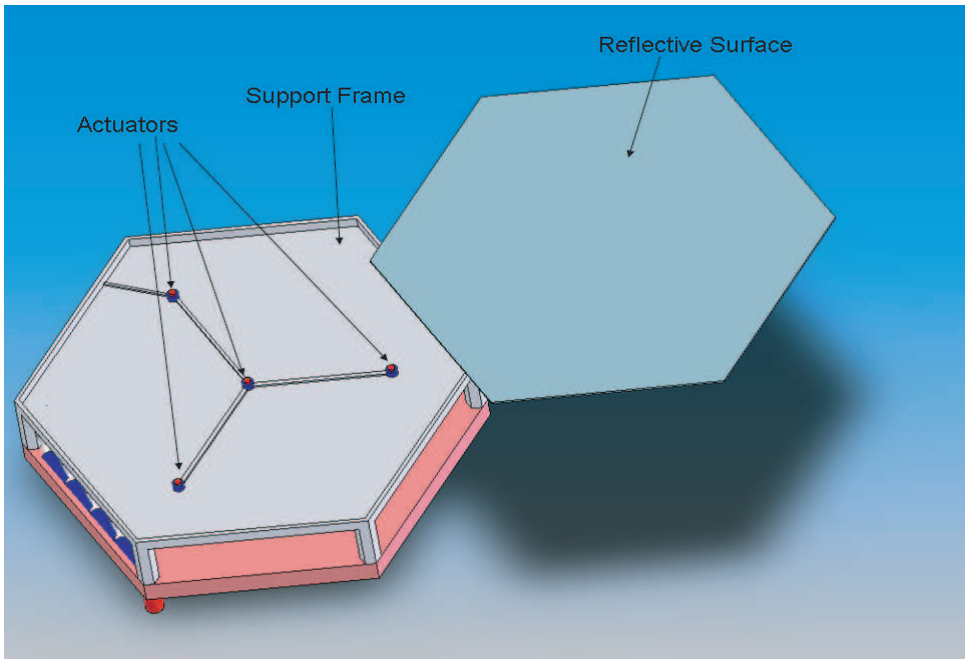

Figure 4.10: Support Frame Actuator Mounting

The geometry chosen for the actuator placement is symmetric with respect to the center point of the mirror thus allowing uniform deformation coverage. There is one actuator placed in the center of the mirror surface that provides the maximum displacement. The other actuators just correct the rest of the surface to the specified equation. This choice for the control system has proven to be the most convenient compromise between accuracy and simplicity of design.

A larger number of actuators would indeed yield a slightly larger precision but also higher cost and a more complex design that could in turn take its toll on the manufacturing processes. The wiring for the control system runs from each actuator to a main feed wire which in turn is coiled under the main support frame and is connected to an outside digital control unit. This setup allows continuous control of the actuator height and correction for any deformations incurred during long term use. A detailed analysis of the control system performance will be provided in the Chapter 5.

4.3 Surface Cooling Subsystem

In order to construct a mechanical system that will withstand high fluctuations in temperature a proper cooling system had to be designed. The laser load applied to the mirror surface is pulsed with a frequency of 10 Hz. The time averaged load on the surface is calculated as 10 Watts per squared centimeter. When taking in consideration the high reflectivity of the mirror surface the load is reduced to approximately 1000 Watts per meter squared. This is achieved by the material choice and also the incidence angle of the incoming rays. The cooling system was designed to keep the optical mirror substrate at a relatively constant temperature thus eliminating the possibility of surface deformation due to thermally induced stresses. Over a long period of time the system will experience certain changes in overall temperature but these will be insignificant as it will be shown in Chapter6.

4.3.1 Sub-System Requirements

The main purpose of the cooling system as outlined before is to maintain constant temperature at the mirror substrate level, but more specific requirements had to

be drawn to ensure the precision of the design. In order to ensure the proper functioning of the optical system the cooling system has to:

- Maintain the mirror substrate at a temperature of 300 degrees Kelvin.
- Be made of flexible piping which can conform to the geometry of the support frame.
- Use water as the cooling fluid.
- Have readily available and relatively inexpensive components.

The above mentioned parameters were taken in consideration in the following sections.

4.3.2 Options for the Cooling System Construction

The main issue that was taken in consideration when investigating different types of piping systems for the mirror was uniformity of surface coverage. For optimum cooling the channels used were placed in the support frame. This frame is thus used as a heat sink for the top surface of the mirror. There were three different conformations investigated for the cooling option.

The first design comprises of a set of rectangular pipes running horizontally from one end to the other of the mirror support frame. An array of fins spans the bottom surface of the support structure to dissipate the excess heat. These rectangular pipes are 6.0 millimeters wide and 2.0 millimeters tall. Water at 280 K enters on one side and exits at about 307-310 K on the opposite side. In order to estimate the effect of such a cooling system the CosmosWorks FEM software package[**?**] was used, since this is a quick and easy way to simulate the

steady state load response of the mirror. The 3D model and the temperature distribution plot are pictured in Figures 4.11 and 4.12.

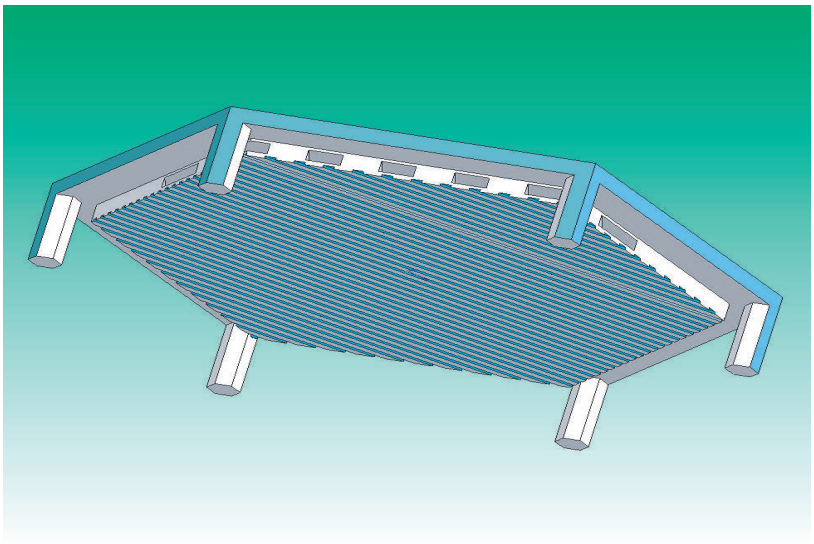

Figure 4.11: Cooling Option 1

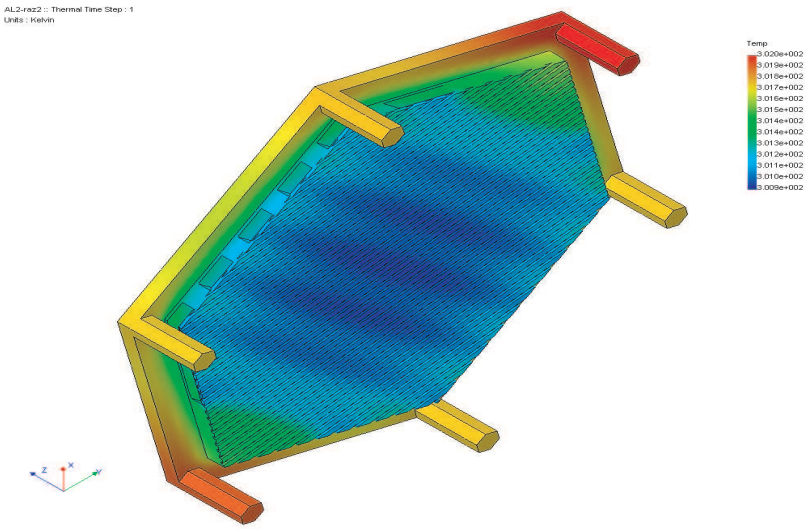

Figure 4.12: Cooling Option 1 Temperature Profile

As seen from the COSMOS plot, the temperature difference throughout the whole structure when withstanding the averaged laser thermal load is about two degrees. The gradient is not enough to cause any significant deformation in the mirror support frame. This cooling option offers a good temperature distribution over the mirror structure.However, the manufacturing issues of drilling rectangular channels of such small dimension through the support frame can render it very costly.

The second cooling option uses circular cross section channels of 4 millimeters diameter. Instead of using straight through channels, this design features channels bent at an angle of 120 degrees. The choice of bent channels was made in order to offer better surface coverage with low temperature areas.

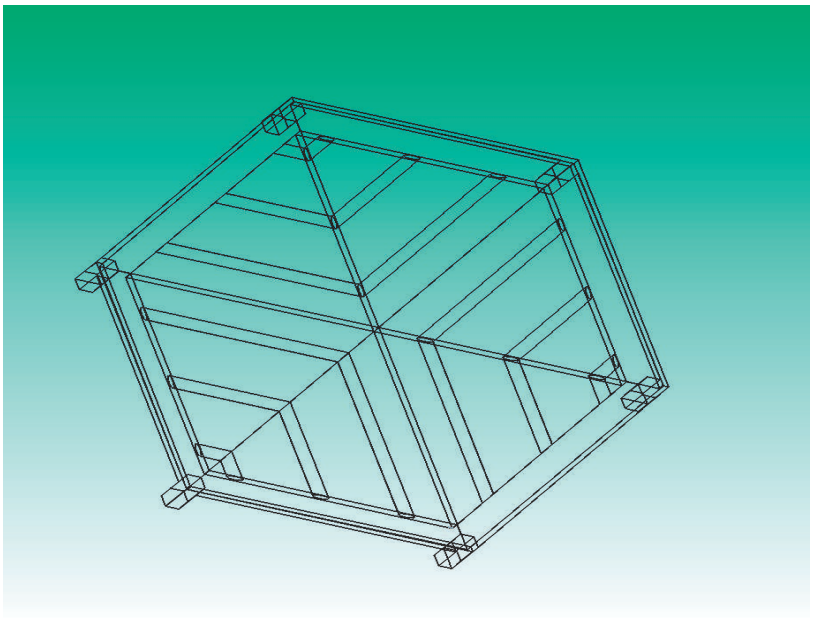

Figure 4.13: Cooling Option 2

The choice of bent channels was made in order to offer better surface coverage with low temperature areas. The symmetrical coverage of the surface shows a

slight advantage. Figure 4.14 shows the COSMOS plot for this cooling choice. The maximum temperature gradient as shown below is much smaller in this

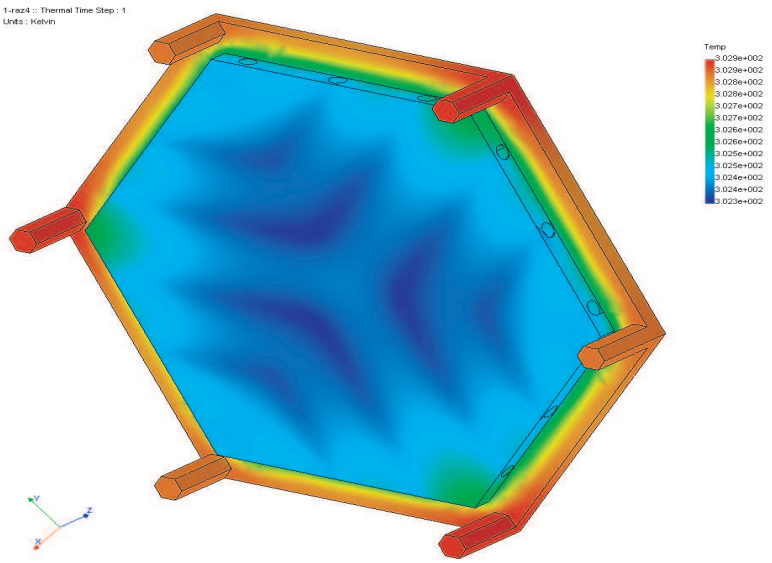

Figure 4.14: Cooling Option 2 Temperature Profile

case; less than one degree. However, the mirror substrate functions at a higher temperature than the first case. From a manufacturing point of view, the second design also has some precarious features since it may be difficult to make the drilled holes meet perfectly at 120 degrees inside the support frame.

The third design option and possibly the most simplistic one features a set of circular cross section channels placed in the same manner as the ones in the first design choice. The drilled channel are 4 millimeters in diameter and they are spaced out 10 millimeters apart. From a manufacturing point of view Design Choice 3 is the easiest and most economic to manufacture. A simple drill with a 4 mm diameter can be used to produce the channels. In spite of the simplistic design the third design performs just as well as the previous two. Figures 4.15 and 4.16 illustrated the 3D model and the temperature response of this design

choice. The temperature profile shown in Fig. 4.16 exhibits a similar temperature gradient to the one shown in Design Choice 1.

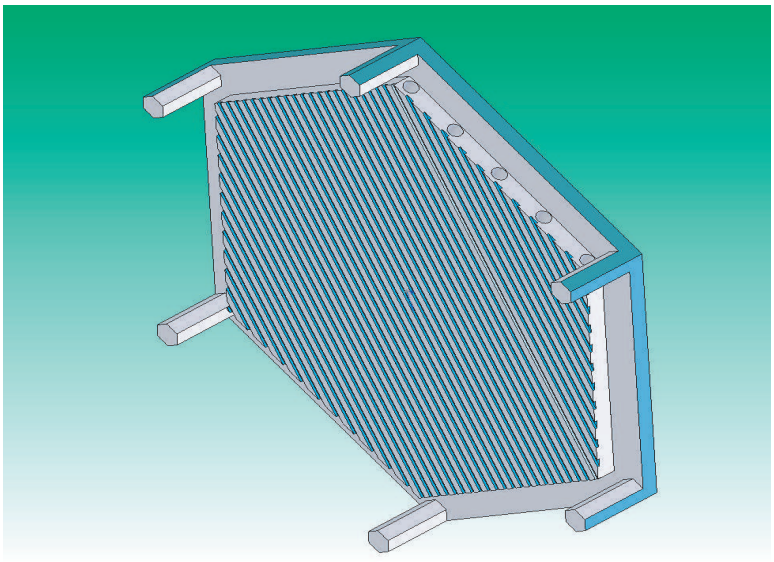

Figure 4.15: Cooling Option 3

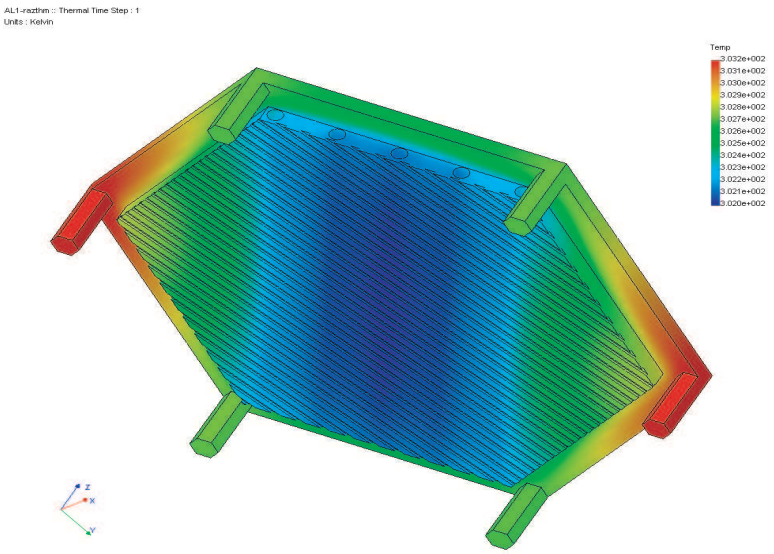

Figure 4.16: Cooling Option 3 Temperature Profile

Although the temperature distribution over the surface or the mirror is not as even as in the previous designs, the temperature difference is about 1.2 degrees Kelvin. The stresses due to this difference in temperature are not going to have a significant effect on the surface profile of the mirror. After evaluation all three design choice the third one seems to be the most advantageous. It is much easier to manufacture than the other two and offers a plausible temperature distribution for the UCLA Final Optics.

4.3.3 UCLA Individual Mirror Surface Cooling System

As mentioned above the cooling option will be straight cylindrical channels. Now, a piping system has to be chosen in order to bring the cold water in and remove the hot water. A set of small curved pipes has been chosen for this task. These pipes have a 4 millimeter diameter and will preferably made from a flexible material. This will allow the pipes not only to bend under the geometrical constraints but will also be able to expand and contract under heat loads. These pipes will fit into the cross drilled channels of the mirror support structure. Once

Figure 4.17: Piping for Option 3 Cooling

integrated into the cooling system these inlet-outlet pipes will be connected to each other by straight small pipes and the resultant flow will be merged into a larger pipe drilled into one of the support pillars of the frame. Figure 4.18 shows the complete integration of the cooling system into the mirror assembly. After

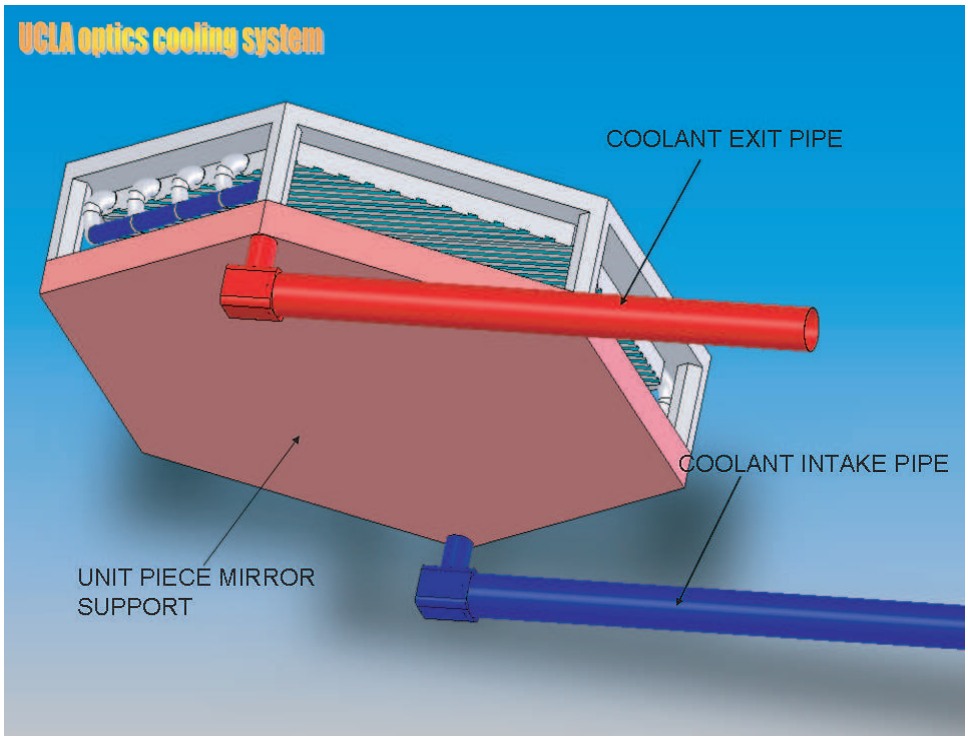

Figure 4.18: Complete Unit Piece with Cooling

the coolant is delivered to mirror structure it is then collected on the other side of the surface. From there the exhaust coolant is pushed into larger pipes under the whole mirror component. The large blue pipe brings the cold water in and the red one collects the hot water and sends it into the exhaust system. The illustration above shows the finished unit piece mirror component of the UCLA Final Optics Design. Using this design as the basic component,the entire large surface mirror can be constructed. The large mirror surface contains 91 unit piece mirrors.

4.4 Large Mirror Assembly

In order to construct a large segmented mirror with almost 100 pieces, a lot of work had to be invested in system integration. In order to make this possible the individual unit segments were constructed in a highly replicable manner. This way integration of two or more unit segments was easily made. As shown in Figure 4.19 the unit segment has its own mounting stand. Therefore by joining all these stands together a large mirror of any shape or size can be constructed. This unique feature allows the UCLA Grazing Mirror Design to withstand any future changes to the large mirror surface configuration. Figure 4.219 illustrates

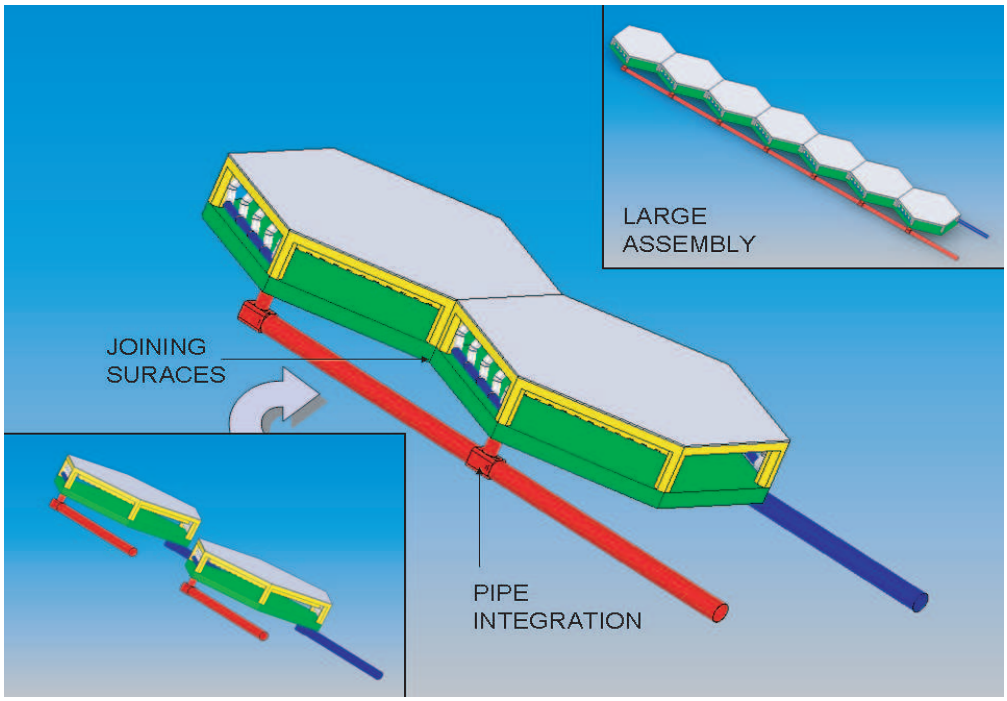

Figure 4.19: System Integration of Unit Segments

the unit-segment joining method. First, the segments are lined up one behind the other both facing up. Next the surfaces on the mounting stand facing each

other are joined. Finally the coolant pipes are connected thus creating a delivery channel from an outside source to the piping inside the mirror substrate. Note that no actual joining has been performed on the support structure for the optical surface or the optical surface itself(as shown, only the mounting stands are joined together). This allows for higher flexibility of such key components in a high thermal loads environment. The large mirror assembly was built from rows of such segments as shown in the above figure. Two separate halves were constructed first;each made up of 40 unit segments. One half of the entire assembly is shown below in Figure 4.20.

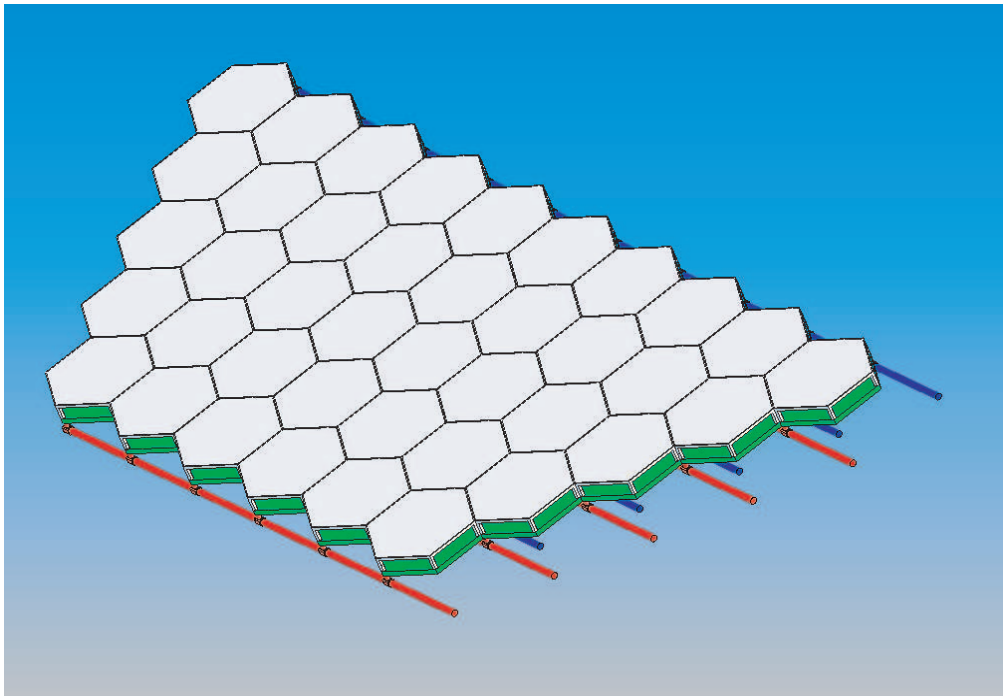

Figure 4.20: Half Piece of Mirror Assembly

A row of 11 unit segments was then inserted in between the two halves. These components were then joined together to form the entire mirror assembly. The total surface that resulted was a hexagonal shaped mirror made up of 91

segmented mirrors with a diameter of 840 millimeters. Once the mounting stands were joined, all the piping was also connected with the ends of the intake and exhaust pipes extended at one end of the large mirror. The two types of pipes were then collected separately into two other pipes which were lead to an external cooling system. Each half of the large mirror has its own collection channel as seen from Figure 4.21. Once the collection channels were mounted on the two

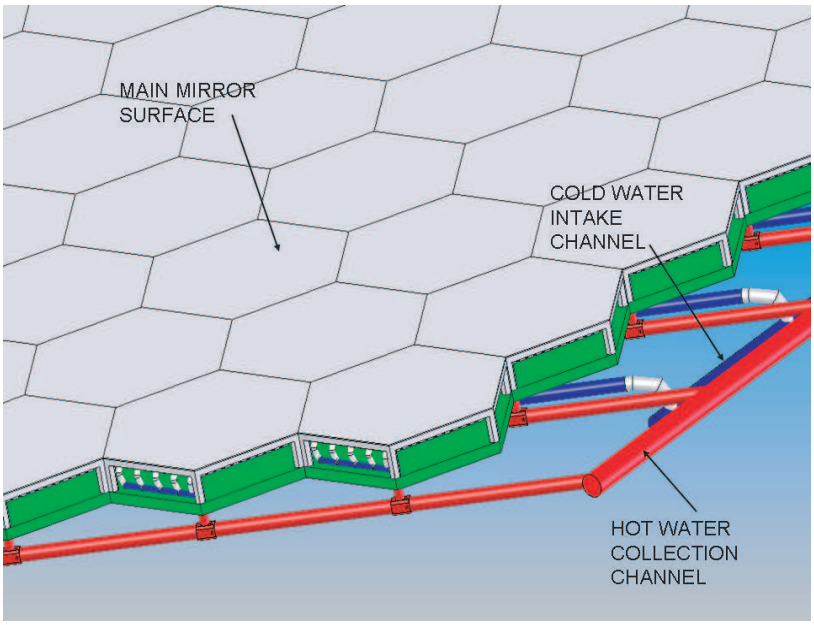

Figure 4.21: Coolant Collection and Intake Channels

halves, the joining of the entire mirror was done. The choice for individual was picked in order to keep coolant pressure drop low within the system. Having less pipe length for the coolant to flow through helps keep the circuit efficient and running at a lower temperature. Figure 4.22, on the following page shows a front view of the entire mirror assembly with the cooling system connected. To better illustrate the complexity of the design, a back view of the mirror assembly with the back casing removed is offered in Figure 4.23. This figure shows a clearer path

of the two different cooling systems. Once the design of the mirror assembly

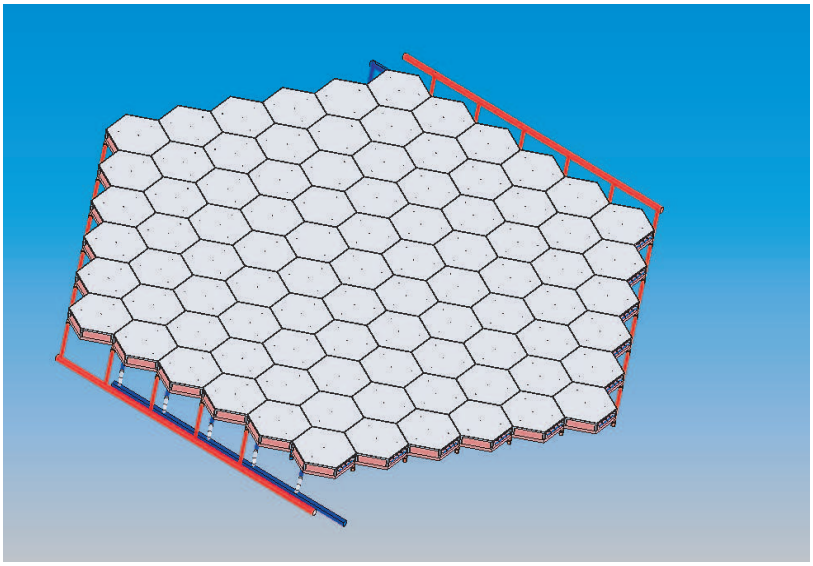

Figure 4.22: Large Mirror Assembly-Front View

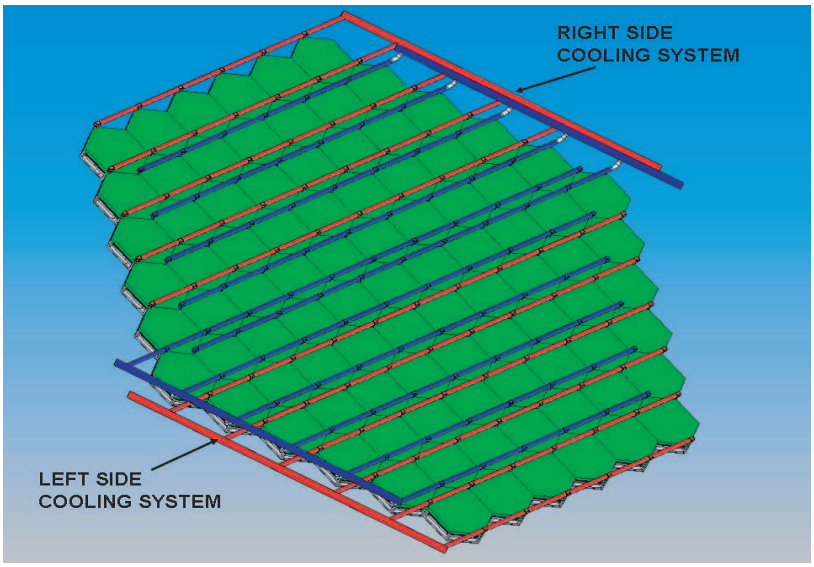

Figure 4.23: Large Mirror Assembly-Back View

was finished, a support system that can sustain its weight was designed.

4.5 UCLA Final Optics Support System

The UCLA Final Optics support system not only needs to hold the mirror's weight but it also should make it possible for the mirror surface to be re-oriented into virtually any direction. This will allow the 64 mirrors necessary for the Inertial Fusion Process to be placed around the Fusion Chamber in a symmetrical manner and then be oriented towards the target. A simple diagram of the mirror placement around the target is offered below.

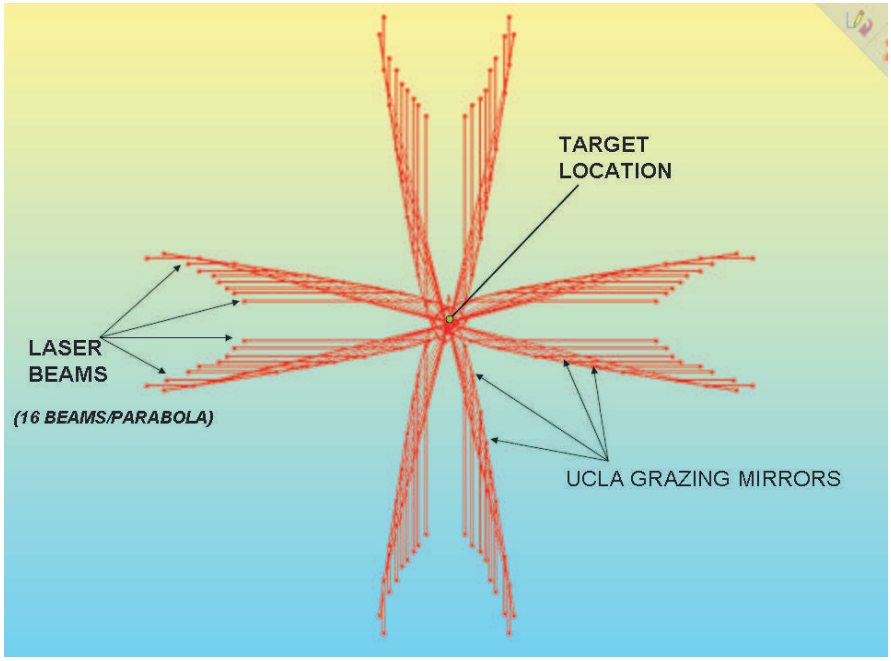

Figure 4.24: Mirror Placement around Taget

The most successful support system has been observed in the past in parabolic antennaes designs. Therefore a similar concept was used in for this part of the UCLA Final Optics.

4.5.1 Sub-System Requirements

The basic mechanical requirements of the UCLA Support System can be identified as follows:

- Be able to support a mass of 250-300 Kg(based on an estimate of the system mass).
- Allow for 180 degree rotation of the reflective surface.
- Be at least 4.5 meters tall(the target is suspended at this height).
- Material of choice should be high strength and low cost.

4.5.2 UCLA Final Optics Support System

Based on the above mentioned requirements a few different designs were investigated. Details about the other support frame choices will shown in Appendix 3. The winning design however, was very similar to that of today's high strength parabolic antennaes stands. It stands 6.2 meters tall. This way the mirror surface is raised to the target level. The material of choice was evidently high carbon steel, which provides stiffness and strength to the structure. The mirror was then mounted on top of the support system and was connected to the rotating frame placed on top. This is the feature that allows the mirror to be oriented towards the target. A swivel-type frame was used on top of the support structure and it was adapted to the mirror shape in order to fit as a circumscribed circle around the hexagonal mirror. The mobility of the frame is 180 degrees in the horizontal plane and 90 degrees in the vertical plane. A figure of the integrated deformable mirror into the support structure is shown on the following page. By integrating

the above mentioned features the UCLA Support System successful satisfaction was shown for the UCLA Deformable Grazing Mirror design requirements.

Figure 4.25: UCLA Design Support System

CHAPTER 5

Material Selection and Laser Damage

The materials choice is a critical feature for the UCLA Grazing Mirror Design due to the fact that an optical surface is t play. Most of the focus is thus turned towards the reflective surface of the mirror. Secondly, material selection was made for the flexible piping used for the cooling system. Individual system unit mounting stand and whole mirror support structure followed. This chapter will also offer a description of the kind of damage to be expected at the mirror surface level. The methodology to make such calculations was developed by Dr. James P. Blanchard.

5.1 Material Selection for Reflective Surface

In order to minimize energy absorption at the mirror surface level due to the laser pulse the UCLA Grazing Mirror Design uses a low incidence angle of the incoming beam. Furthermore, to further reduce surface heating and thus damage to the mirror a finely polished highly reflective material was chosen. The search was narrowed down to pure aluminum layer as the mirror face. The reason for this choice was mainly the fact that reflectivity of Aluminum stays relatively constant around 95 percent regardless of the laser wavelength. The graph on the following page, excerpted from the HAPL Final Optics web-site, alludes to this matter. The plot[**?**] shows reflectivity of materials in the case of perpendicular

incidence; although the UCLA Design uses a shallow angle which further reduces the potential surface damage. It can also be observed that two other metals have even higher reflectivity than Aluminum, Silver and Gold respectively. Although these metals would be good candidates, they lack versatility when it comes to change in laser wavelength.

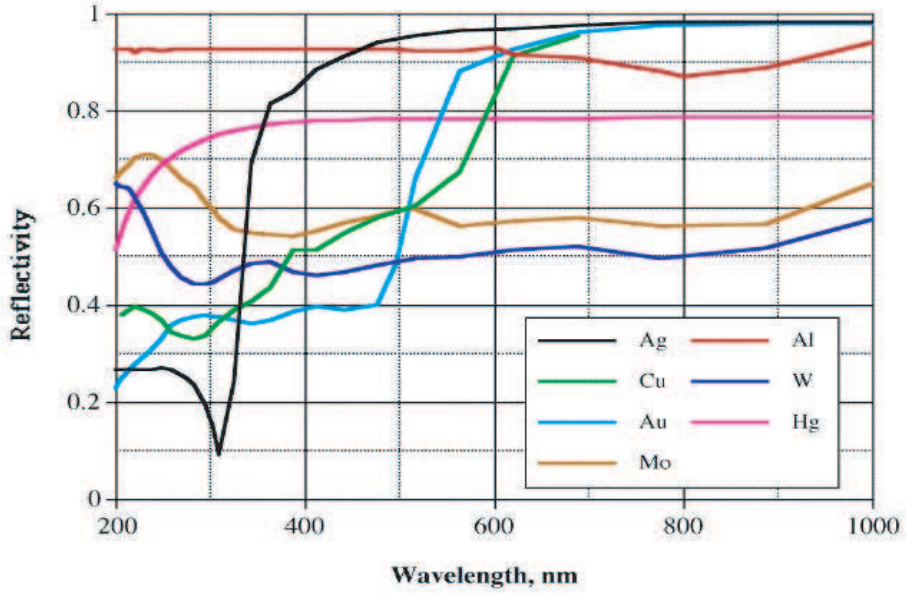

Figure 5.1: Metal Reflectivity versus Laser Wavelength

They achieve high reflectivity (about 98 percent) only in the 600-1000 nm wavelength range. Therefore in case of lower wavelength laser they would absorb significant amounts of energy, whereas Aluminum stays at 95 percent for a wider range. Another concern, not necessarily less important in the selection process was cost. As shown before there are 64 large mirrors each measuring almost one meter in diameter to be covered with the reflective metal. Using Silver or Gold for such a task could become expensive. The substrate material of choice was Aluminum 6061. This is high strength, low thermal expansion material[**?**].

Table 5.1: Properties of Aluminum 6061

Properties, Value	
Density	2700 Kg/m^3
Poisson's Ratio	0.33
Elastic Modulus	80 GPa
Tensile Strength	125 MPa
Yield Strength	55 MPa
Thermal Expansion Coefficient	23.4e-6 /K
Thermal Conductivity	240 W/m/K
Thermal Diffusivity	84 e-6 m^2/s

Table 5.1 shows the mechanical properties of this material. The high tensile strength will allow the material to sustain induced thermal stresses due to the laser pulses. Also, the low coefficient of thermal expansion will prevent high deformation to the mirror surface. These properties will be later on used in the Analysis section of the thesis.

5.2 Material Selection for all other Systems

The flexible piping used for the cooling system is also a very important feature to design. The material for these pipes has to not only bend around the structure but also be able to withstand temperature variations. For this task, a PVC compound can be used. PVC is a highly versatile material that can be designed for different application. This allows it to work smoothly with the requirements of the UCLA Design Cooling System. The temperatures that the piping system has to withstand are between 290 and 310 degrees Kelvin. The gradient will not

Table 5.2: General Properties of PVC

Properties, Value	
Tensile Strength	2.60 N/mm^2
Thermal Expansion Coeficient	80 x 10-6 /K
Density	1.38 g/cm^3
Tensile Strength	125 MPa
Max Cont Use Temp	60C^o

Table 5.3: Important Properties of Copper

Properties, Value	
Tensile Strength	400 MPa
Yield Strength	250 MPa
Density	8900 Kg/m^3
Thermal Expansion Coefficient	2.4e-5 /K
Thermal Conductivity	390 W/m/K
Specific Heat	390 J/Kg/K

be large enough to cause any damage to the tubes. Table 5.2 shows the general PVC properties[**?**][**?**].

For the support structure of the unit segment of the mirror, the best candidate seemed to be Copper since it has high thermal conductivity. This feature is important since the mirror surface comes in contact with the Copper stand.

Flexible piping segments are also enclosed in two of the legs of the support structure(see Figure 5.2). Table 5.3 contains important properties of the Copper Alloy used for the support frame[**?**]. For the mounting stand that holds the support frame for the mirror surface the material of choice was Steel Alloy

AISI1020[?]. A sheet of this material, 0.005 m thick will be inserted as the main mounting stand for the large mirror surface. As seen from the modelling section this sheet will have a hexagonal shape. The Steel Alloy will also be the material of choice for the large support structure that holds the UCLA Optics design oriented towards the target chamber. This material option satisfies the system requirements outlined in Section 4.5.1 for the mirror stand. All the other components of the UCLA Final Optics Design, such as bolts, actuators and fittings will be obtained from commercially available sources. Therefore, their material constitution will be dictated by the manufacturer.

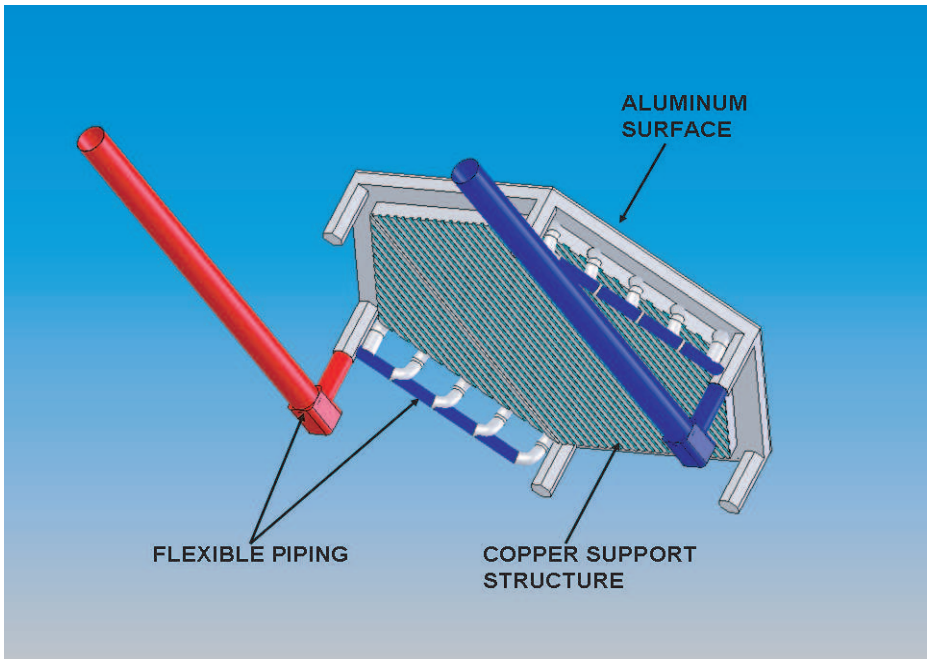

Figure 5.2: Mirror Unit Segment (no mounting stand)

Table 5.4: Important Properties of AISI1020

Properties, Value	
Tensile Strength	420 MPa
Yield Strength	350 MPa
Density	7900 Kg/m^3
Thermal Expansion Coefficient	1.5e-5 /K
Thermal Conductivity	47 W/m/K
Specific Heat	420 J/m/K

5.3 Surface Laser Damage

The effect of laser beams on reflective surfaces has been always investigated for many reasons. It is important to know what kind of surface defects can be produced due to a high power laser shots. The damage threshold of optics for use with true pulsed lasers such TEA CO2 lasers is expressed in units of Joules/cm2, at a given pulse length. It is difficult to scale this figure for damage threshold to account for different pulse lengths, but there is some correlation that the figure varies with the square of the pulse length. So for a pulse twice as long the damage threshold in units of J/cm2 is four times greater. This section focuses on two significant literature surface pertaining to damage sustained by Aluminum surfaces due to laser pulses. The first paper,"UV LASER-INDUCED DAMAGE TO GRAZING INCIDENCE METAL MIRRORS"(by M. S. Tillack, J. E. Pulsifer and K. Sequoia), outlines two kinds of defects caused at the surface of Aluminum mirrors. The damage shown was sustained after only 50 shots on a polished Aluminum mirror at 5 J/cm2 in vacuum. First, grain separation is clearly evident. Grain movement can occur from differential thermal stresses across neighboring

grains.The figure below, excerpted from the above mentioned publication, shows grain separation and slip line transport.

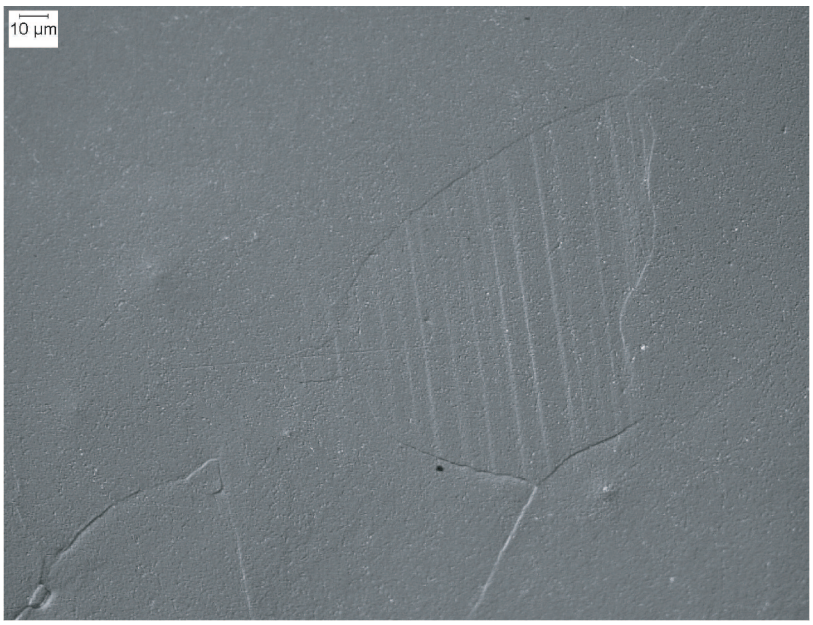

Figure 5.3: Polished Aluminum Surface Damage

The process of mechanical polishing appears to stimulate grain boundary effects by introducing impurities and stresses into the system. Secondly,as mentioned, there is also clear evidence of slip line transport. These defects concentrate in slip lines which eventually emerge as ordered roughness at the surface.[**?**] It was also mentioned that a better result might be obtained from diamond turned surfaces. Other types of milder damage would be surface swelling and surface spotting(isolated high temperature areas).

Another important paper that clearly shows damage results to Aluminum surfaces is "Damage Threats and Response of Final Optics for Laser-Fusion Power Plants" by M. S. Tillack, S. A. Payne and N. M. Ghoniem. Experimental data from Dr. Tillack's paper mentioned above is described briefly below. Experiments

were performed using a frequency-doubled YAG laser with a beam size of 1.2 cm and maximum energy of 800 mJ.Mirrors were fabricated by diamond turning 99percent pure (Al-1100) and 99.999 percent pure Aluminum with a natural oxide coating 30 nm thick[?]. The experiments were performed for single and multiple shots up to 104, all at 85 angle of incidence. The Al-1100 mirrors survived single shot exposure up to 18 J/cm2 normal to the beam. Below 8 J/cm2 no visible damage is observed up to the maximum number of shots tested. The figure below shows an Al-1100 blank before and after 104 shots of 20 J/cm^2.

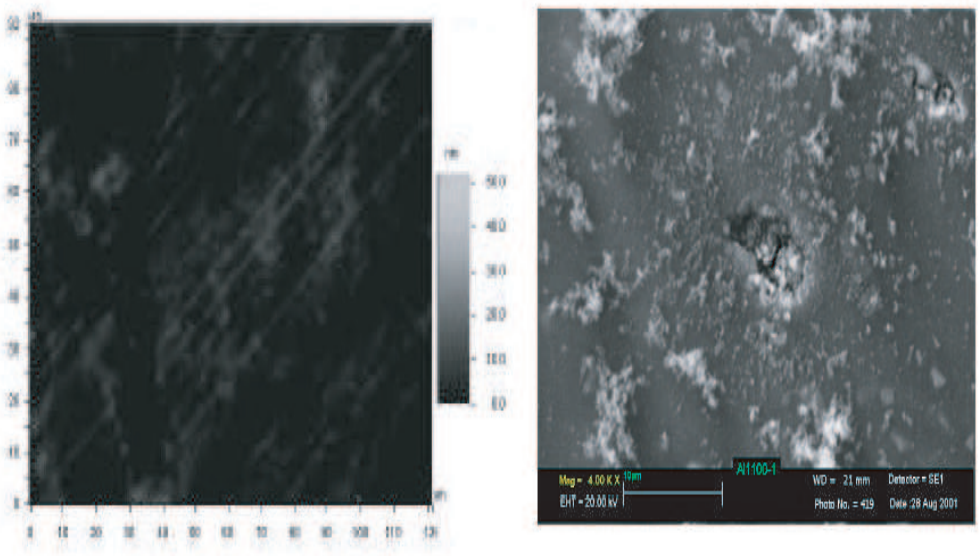

Figure 5.4: Laser Damage to Aluminum Surface

While experiments are still ongoing an estimate of the safe range of laser power was done. This is important to appreciate since the optical surface has to obey very strict parameters in order to function properly. Figure 5.5 on the following page shows a graph that was excerpted from the same publication by Dr. Tillack. It is obvious that for Aluminum the optimal surface load should be below 10 J/cm^2. Therefore, this value will be used for the steady state analysis

described in the next chapter.

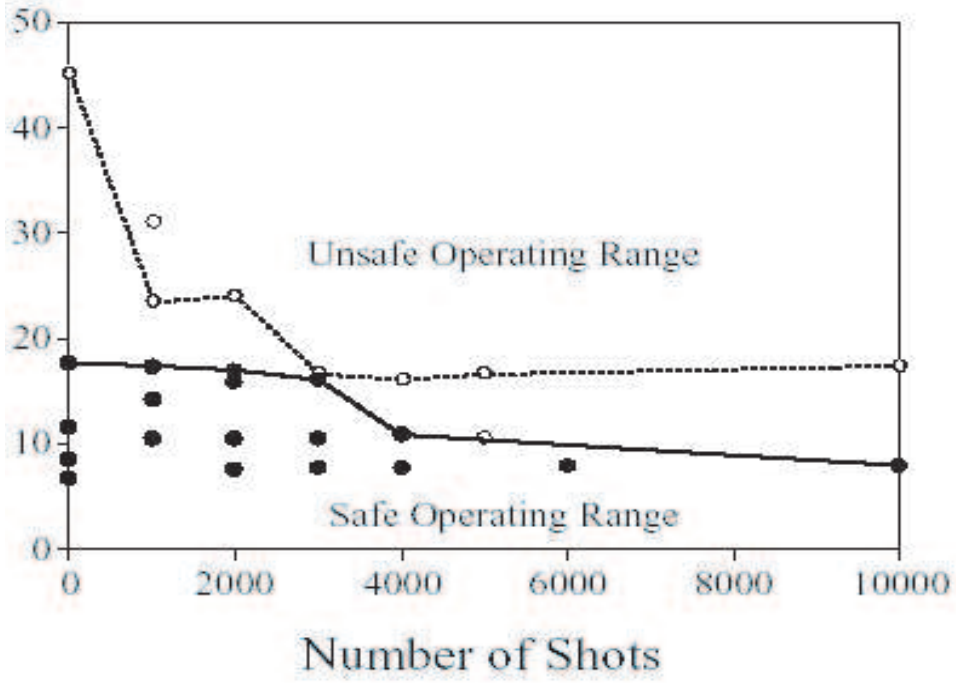

Figure 5.5: Laser Power vs. Number of Shots

CHAPTER 6

Design Approach and Results

The UCLA Design was shown so far to have a well structured mechanical system and a compatible material selection. After all design work was finalized, every system had to be analyzed for performance. This section will show in detail all the analysis results obtained from investigating the optical performance, steady state response and transient design as well. The optical performance analysis was performed by running a set of static and dynamic simulations[**?**] on the mirror surface alone in order to mimic the function of the piezo-electric actuator. The steady state analysis was performed on the entire unit of the UCLA Final Optics design including cooling channels and mirror surface. In this case an analytical estimation a COSMOS[**?**] simulation and an ANSYS run were compared to ensure accuracy and validity of the results. The transient thermal and stress analysis was executed only using ANSYS and is considered to be the more significant thermal stress response pertaining to the UCLA Design.

6.1 Optical Design and Precision Results

This section will demonstrate the capability of the UCLA Design as a reflective and focusing surface for the Inertial Fusion Process. The deformable Aluminum surface of the unit segment was selected. As shown before, this surface is a hexagonal piece with a radius measuring 50 millimeters and 1 mm thick. In order to

show the functionality of this surface a series of simulations was performed. First the model was deformed in conformity with the displacement specifications dictated by the mathematical surface. The resulting forces on the back surface were then obtained. Secondly, the forces obtained in the fist step were applied to the actuator location and the deformation was observed. The resulting displacement were this time collected and documented. Thirdly, a comparison between the theoretical and practicably obtainable displacement was conducted and an error estimation was made. The starting configuration was a hexagonal piece selected from the parabolic surface. The distance from the center of the hexagon to the focal point measured 15 meters. The four actuator's positions are shown in the

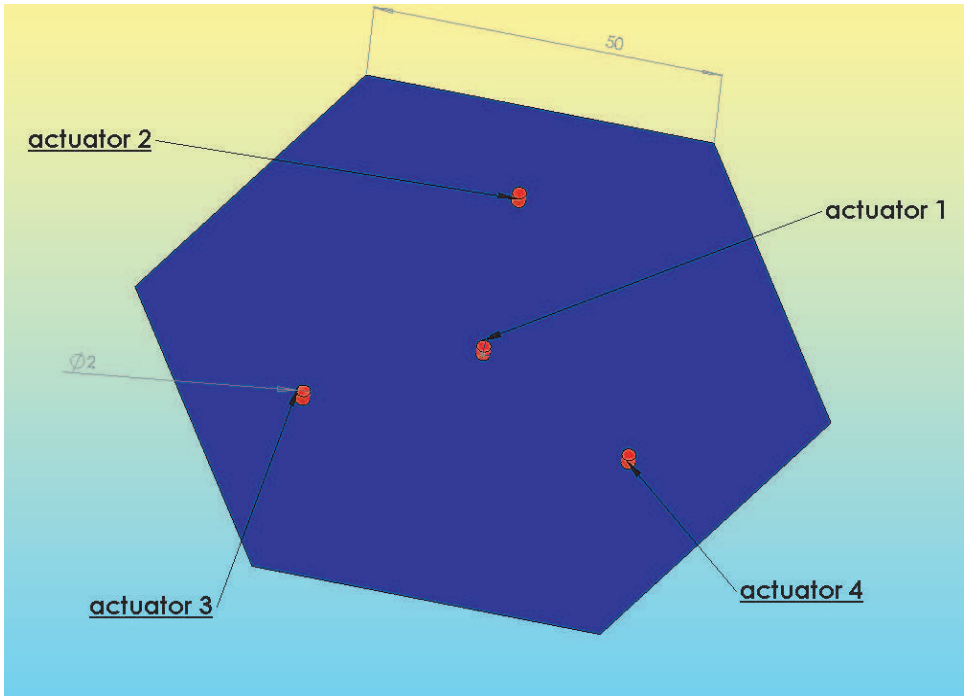

Figure 6.1: Placement of actuators on backface

Figure 6.1 above and they are numbered 1 through 4. The coordinates for these points were obtained from the paraboloid equation accordingly. Table 6.1 shows

Table 6.1: Coordinates of Actuators on Paraboloid

Actuator number, X-coord, Y-coord, Z-coord			
1	13.5 m	5.196152 m	0 m
2	13.511500 m	5.199961 m	0 m
3	13.488500 m	5.194200 m	0.025 m
4	13.488500 m	5.194200 m	-0.025 m

the coordinates of the four actuators on the parabolic surface.

Equations 4.1 and 4.2 were used to obtain the above mentioned coordinates. Once the locations of the prescribed points on the paraboloid surface was established, their locations on the undeformed Aluminum mirror had to be identified. The following figure shows a side view of the undeformed surface and the final profile to which it needs to be conformed. The spatial coordinates of the actuating

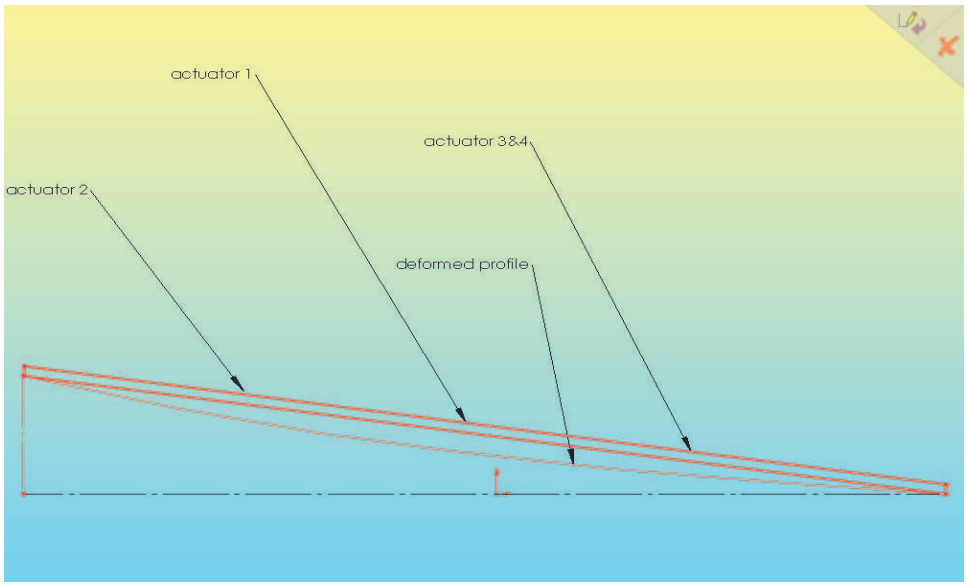

Figure 6.2: Side view of undeformed and deformed mirror

Table 6.2: Coordinates of Actuators on Mirror Flat Surface

Actuator number, X-coord, Y-coord, Z-coord			
1	13.5 m	5.196038 m	0 m
2	13.511500 m	5.199872 m	0 m
3	13.488500 m	5.194121 m	0.025 m
4	13.488500 m	5.194121 m	-0.025 m

points on the flat surface of the mirror are shown in Table 6.2.

By investigating the two coordinate tables, the displacements necessary for the points on the flat surface to move to the paraboloidal surface can be easily calculated. These conditions would be applied to the four actuators in order to achieve focusing. Notice that the change in coordinates is only registered in the Y direction. This condition was imposed when designing the surface due to the fact that the actuators are the push-pull type thus limited to one direction. The required displacements for each point are as follows:

- Actuator 1 Displacement Δ=0.0001138 m.
- Actuator 2 Displacement Δ=0.0000879 m.
- Actuator 3 Displacement Δ=0.0000787 m.
- Actuator 4 Displacement Δ=0.0000787 m.

The displacements shown above were imposed on the mirror surface by running a static analysis program in ANSYS. The properties of AL 6061 were used in the analysis. The hexagonal surface was then constrained at all six corners with zero displacement in the Y direction(Z in the coordinate system of the FEM

software). The displacements were then applied to the points corresponding to the actuators positions on the back surface. The mesh applied to the surface in this case was very fine in the plane of the surface itself since the relative positions and forces on these points is were more important than those across the thickness. Moreover, further refinement was done to the area inscribed between the actuators to ensure that the obtained results would be as accurate as possible. As it can be seen from above, a slightly different model had to be constructed

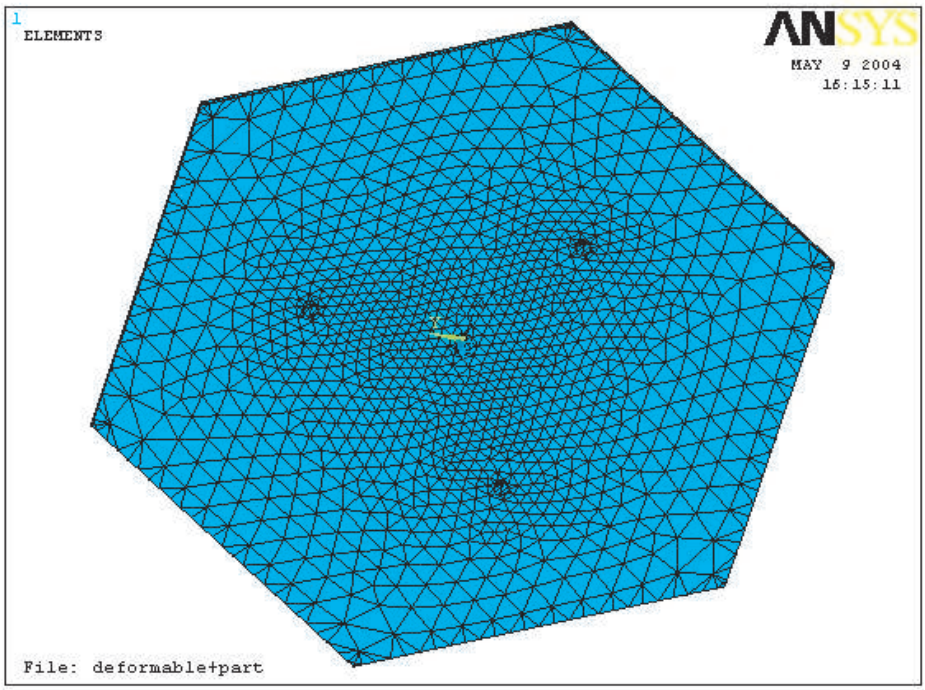

Figure 6.3: Meshing of Mirror for Focusing Analysis

having protrusions on the back surface to mimic the actuator body, even though these are not literally attached to the deforming surface. The ambient temperature was set to 305K for this particular run to simulate steady state functioning conditions of the mirror. A plot of Z direction displacements of the mirror surface resulting from the static analysis is shown in Figure 6.4 on the following page. It

can be easily seen that the surface is pulled unevenly with respect to the center of the mirror. This is a result of the surface equation which describes an off-axis

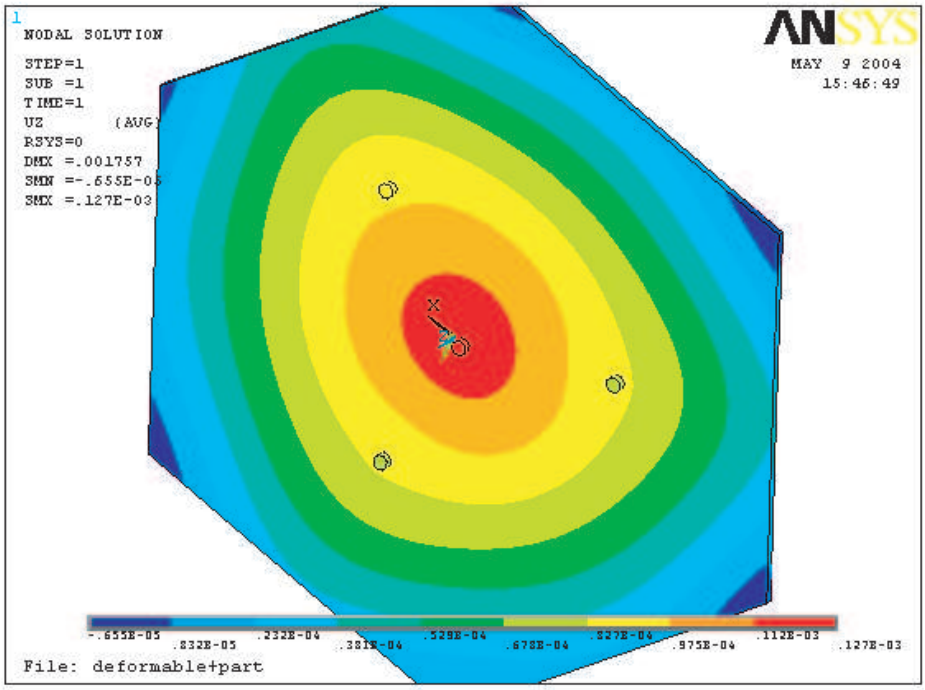

Figure 6.4: Displacement Plot of Deformed Unit Mirror

segment of the focusing parabola. Therefore, the displacement should indeed be nonsymmetric with respect to the center. The resulting forces exerted on the mirror were also extracted from the FEM analysis. The forces of interest were the ones felt by the actuating points in the Y (Z for the model) direction. They are as follows:

- Actuator 1 F_z=3.02 N
- Actuator 2 F_z=2.2 N
- Actuator 3 F_z=2.0 N

- Actuator 4 F_z=2.0 N

Once the resulting forces were obtained, a new FEM program was run to simulate the application of these forces. In this program, the corners were again fixed in the Z direction and forces applied to the actuators. The following figure shows a plot of the resulting displacements in the Z direction due to those forces. It is easy

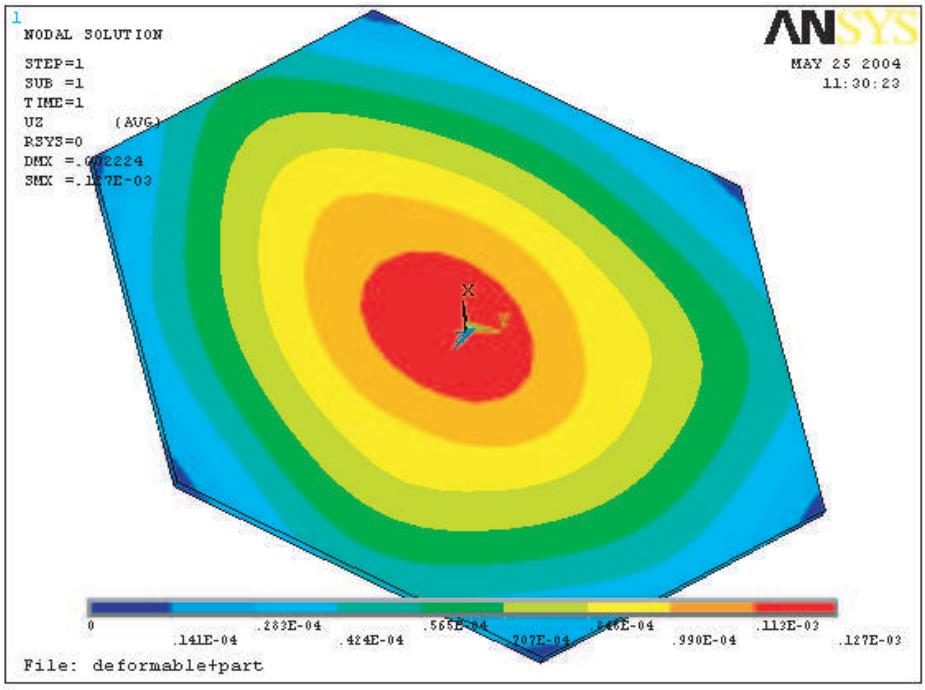

Figure 6.5: Displacement Plot of Deformed Unit Mirror

to observe that this plot is very similar to the one shown on the previous page. This ensures the accuracy of the applied loads. Extracting the displacements for the actuating points the following results are obtained:

- Actuator 1 Displacement Δ=0.000121877 m.
- Actuator 2 Displacement Δ=0.000090765 m.

- Actuator 3 Displacement Δ=0.000084875 m.
- Actuator 4 Displacement Δ=0.000084496 m.

The focusing error can now be calculated. The individual measurement error for each actuator were fairly small compared to the expected values. Actuator 1 (center) experienced a 6.6 percent margin of error;actuator 2(top) yielded an error of value of 3.1 percent and actuators 3 and 4 (bottom) showed an approximately equal error value of 6.8 percent. Using these values the overall surface standard error was obtained as 5.5 percent which is extremely close to the design requirements outlined in the design chapter of the thesis. Of course, the control system would be able to correct of this kind of error if need be, although in practice this might not destabilize the optical system.

6.2 Analytical Estimates of Thermo-mechanical Response

In order to ensure the accuracy of the thermo-mechanical results from FEM analysis, some analytical estimates had to be obtained for the steady state and transient responses. This section,first makes reference to Dr. James P. Blanchard's paper on surface heating, namely "Practical Considerations for Thermal Stress Induced by Surface Heating". Dr. Blanchard's paper starts from the consideration of a model fully constrained in two dimensions and free in the third dimension. This situation is similar to the one presented in the thesis. In the case of surface uniform heating applied on a half-space, Dr. Blanchard estimates the surface temperature as:

$$T_{surface} = \frac{2q}{k}\sqrt{\frac{\kappa * t}{\pi}} \tag{6.1}$$

Where q is the surface heat flux, k is the thermal conductivity and κ is the thermal diffusivity. The stresses associated with a model that is subjected to rapid surface heating then become:

$$\sigma_{zz} = \sigma_{yy} = \frac{-2qE * \alpha}{(1-\nu) * k}\sqrt{\frac{\kappa * t}{\pi}} \tag{6.2}$$

and

$$\sigma_{xx} = 0 \tag{6.3}$$

These estimates are designed for short time surface heating and assume spatial uniformity of the applied heat and it ignores both elastic and thermal waves. The equation of interest is this case is that of surface temperature. Conceptually, this estimate is not very precise since it does not take in consideration volume heating below the surface. This is acceptable in the case of the UCLA Final Optics design since the thickness of the reflective surface is very small. Therefore, it is expected that the actual surface temperature resulting from the FEM analysis conducted using the ANSYS software package will be lower than Dr. Blanchard's estimate. The UCLA final optics design also uses a cooling system which keeps the mirror at a lower temperature than the environment; which will definitely have an effect on the resulting surface temperature. Using Dr. Blanchard's[**?**] equation for temperature estimation it was possible to find the instantaneous surface temperature due to one laser pulse. The following parameters were used when calculating the instantaneous surface temperature:

- Surface heat flux q=2*10^{11} W/m^2
- Thermal Conductivity k=240 W/m/K
- Thermal Diffusivity κ=84 e-6 m^2/s
- Length of Laser Pulse t=5 ns

The resulting surface temperature is 610 Kelvin. As it will be shown in the next chapter, this value is slightly higher than the FEM result. However, the method shown above offers a good prediction for what's to be expected from the FEM analysis. Once a temperature estimate has been obtained it is important to have an idea of the potential laser damage to the mirror surface.

An estimate temperature increase was also obtained for the steady state long term case. The following classical formula was used[**?**]:

$$Q = m * c_p * \Delta T \tag{6.4}$$

The following parameters were used:

- Q=1000 J/m^2
- c_p=900 J/KgK
- Density=2700 Kg/m^3
- Surface Area = 1 m^2

A 99 percent reflectivity was assumed for the calculation of the temperature increase. The resulting value was 2^o C. As it will be shown in the next section, this result is in close conformity with the FEM results. This increase will not have any long term effects on the surface morphology. Therefore, no optical performance degradation is expected.

6.3 Steady State Thermo-Mechanical Analysis

As mentioned at the beginning of Chapter an FEM model was constructed and the steady state loads were applied to it. The load applied was 1000 J/m^2 to the

mirror surface. The mesh chosen for this simulation is unform in all direction. This method was chosen because in the steady state case the heat gets dissipated evenly throughout the whole model.

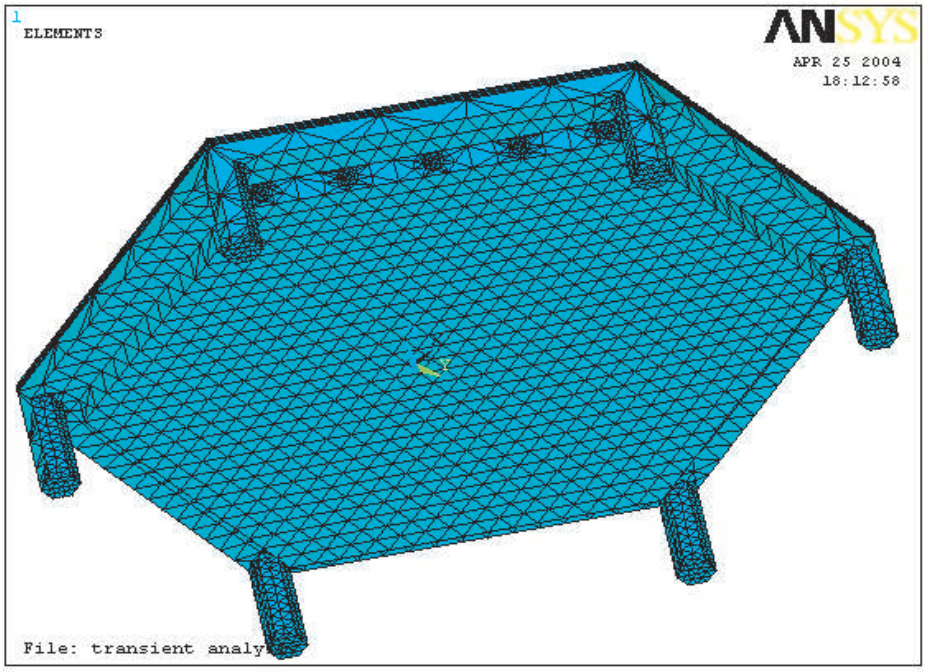

Figure 6.6: Mesh of Unit Mirror Segment

Two different FEM programs were used to come up with the steady state response of the mirror; COSMOS and ANSYS. This was done to avoid any software bias error. Material properties were entered for Copper- pertaining to the support structure and Aluminum-for the reflective surface on top. The COSMOS simulation results were shown in Chapter 4, Cooling System section and it showed a temperature gradient of 1.8 degrees. The ANSYS results also show similar values, which confirm the validity of the simulations. The difference in temperature in this case is about 1.5 degrees. The starting temperature of the system was actually 305 K but the cooling system stabilized it to about 300 K

before the heat load is applied. The thermal plot is shown in Figure 6.7.

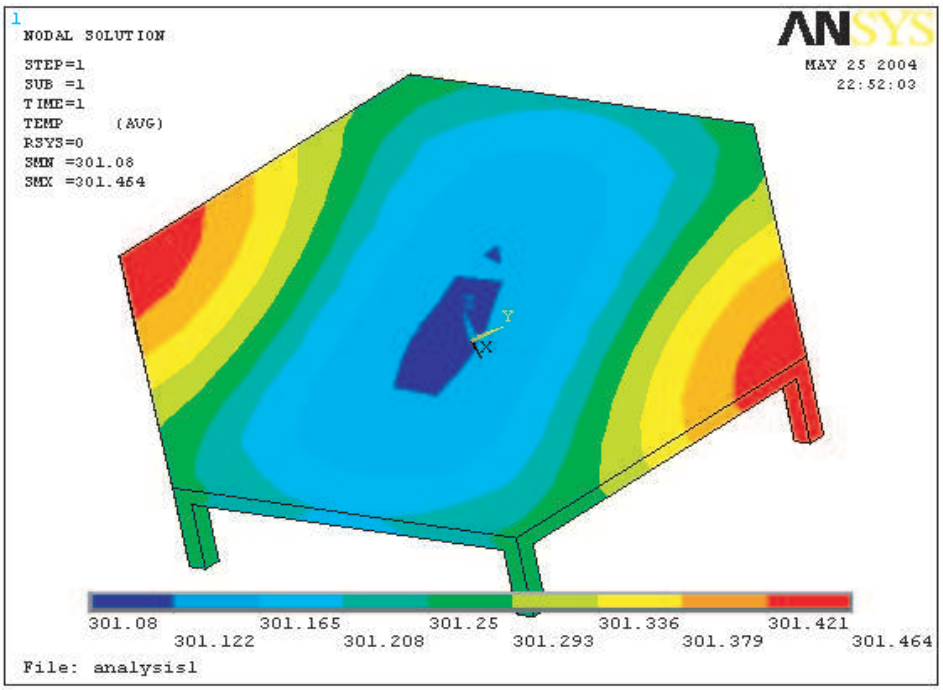

Figure 6.7: Steady State Temperature Response

As it can be seen, the gradient is fairly uneven over the surface. This is due to the fact that the cooling pipes cover mostly the central area of the mirror. It is also obvious that the thermal response for the reflective surface is in concordance with the analytical estimation offered in the previous section(2^oC) Once the thermal analysis was completed, a file with the temperature distribution was created. This file was used to apply thermal loads to the static model. Constraints were then applied to the corners of the reflective surface to simulate joining to the Copper support structure. Only the top surface was used for the mechanical simulation since the Copper structure will withstand minimal thermal stresses.As seen from Figure 6.8 on the next page, the average surface Von Mises stress value is about 25 KPa which is relatively low. There are however, some areas of higher stress

concentrations around the points of support due to the restraints involved. This situation will likely not show up in the real model because the corner constraints will still allow for some movement in the plane of the mirror. Both temperature

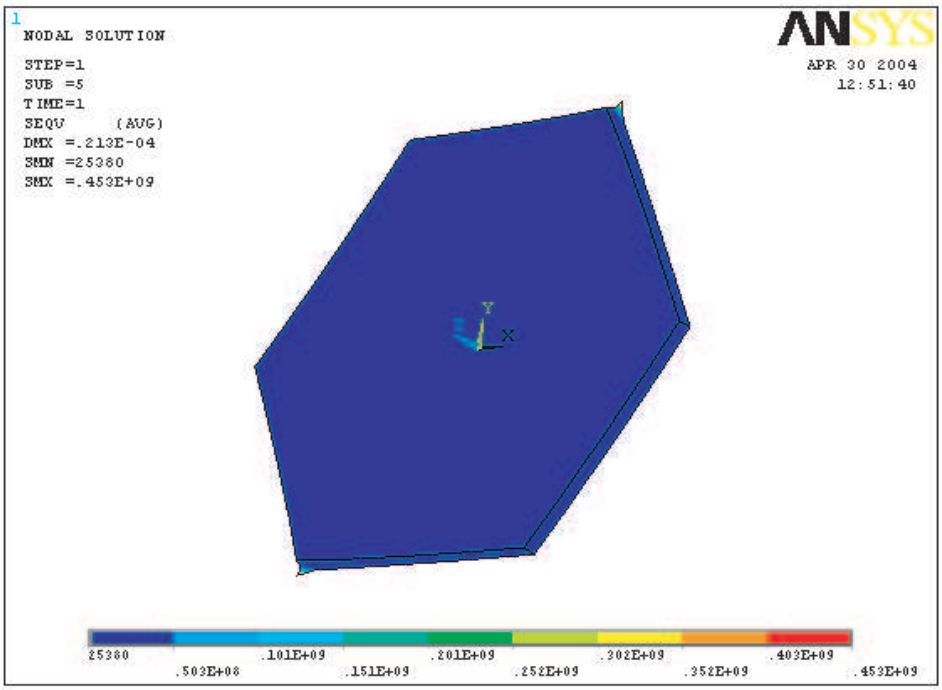

Figure 6.8: Steady State Stress Response

and stress responses outlined in this section show that the UCLA design would function properly under long term-steady state conditions.

6.4 Transient Thermo-Mechanical Analysis

To better understand the conditions under which the UCLA Final Optics design will operate, a more involved type of analysis had to be performed. Only the ANSYS software package was used in this case to run the simulation since it is a more complete transient analysis program than COSMOS. The mechanical and

thermal properties of the materials in this case were entered as time dependent for temperatures between 300K and 700K. The meshing of the reflective surface was also done differently in this case. Due to the higher temperature gradient across the thickness more elements have been created in this direction, while coarser elements were chosen in the plane of the surface. The following figure is a zoomed in picture of one of the corners of the mirror to show the number of elements across the thickness. Notice there are six elements placed along the thickness. This type of arrangement ensured accurate results for the temperature

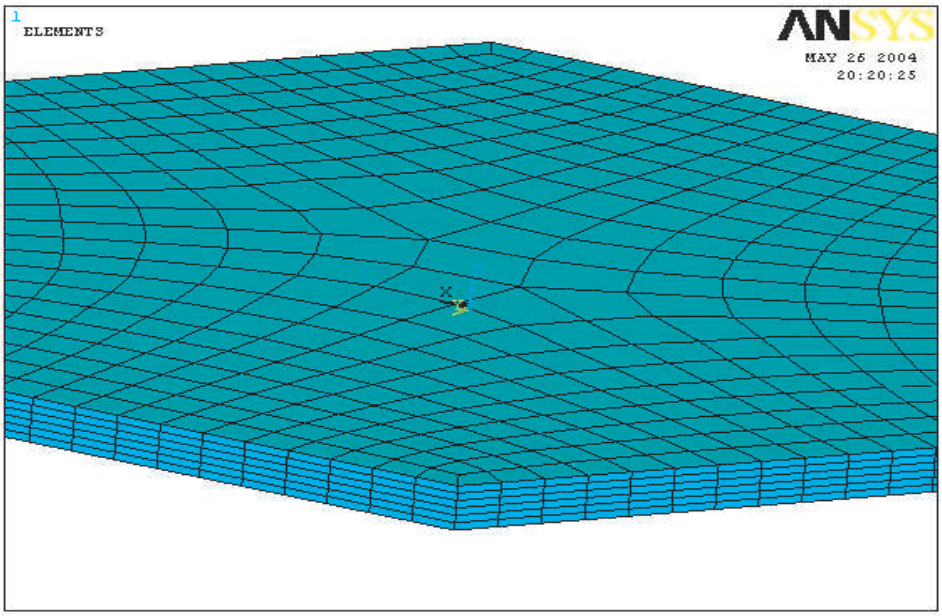

Figure 6.9: Transient Analysis Mesh

distribution. Once the materials and the mesh inputs were set, the actual loading scheme was programmed. From the parameters of the ICF Process a load pulse was set to hit the top surface of the mirror every tenth of a second. Using the load from the analytical study, surface heat flux q=2*10^{11} W/m^2, the mirror was studied for a length of nine pulses. A convective load at 280 K(from water

cooling) was applied to the back of the surface. The initial system temperature was set for room temperature (300K). The transient mode analysis was then run. The resulting temperature behavior at certain depths in the mirror was then obtained. The figure below shows the temperature response of the at the face of the mirror. As it can be seen, the temperature at the surface peaks at

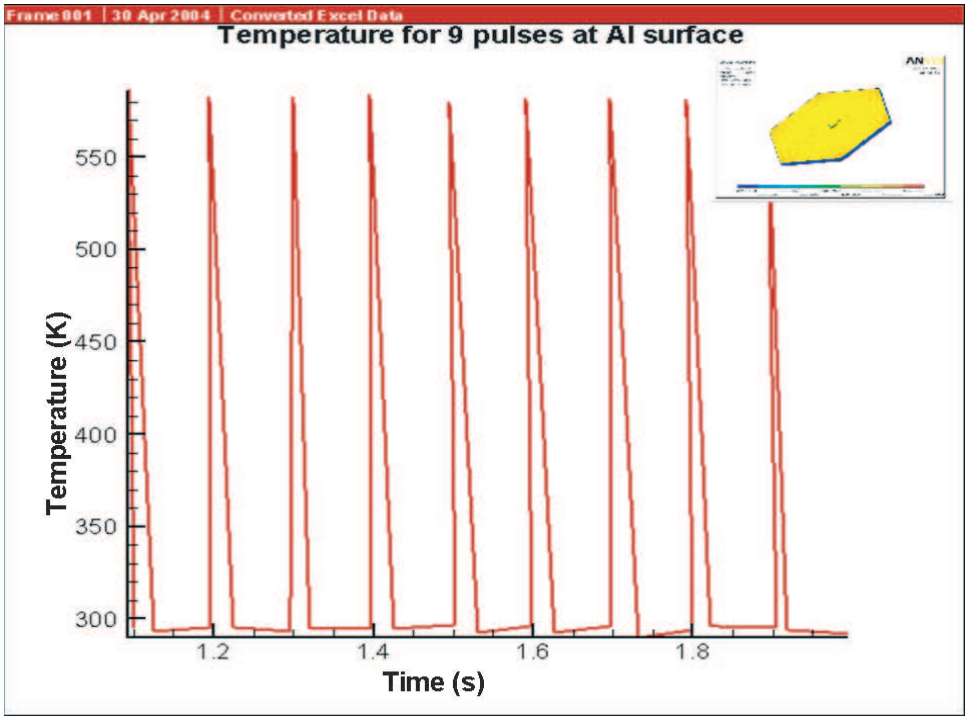

Figure 6.10: Thermal Response for 9 Pulses on Surface

600 K. Despite the drastic temperature increase, the material cools back sown to its initial temperature very fast before the next pulse hits the surface. The temperature increase to 600 K also verifies the analytical results shown earlier. It is seen here that the maximum temperature does not rise to 607 K as shown in the analytical estimate. As mentioned before, this is due to the fact that Dr. Blanchard's estimate does not take in consideration heat dissipation through the thickness on the material. The convective cooling on the back surface is also

not taken in consideration. In order to get a better understanding of the cooling sequence after the pulse hits, a plot of temperature vs. time for one pulse is shown. The thermal response at .05 mm was next investigated(see figure 6.12).

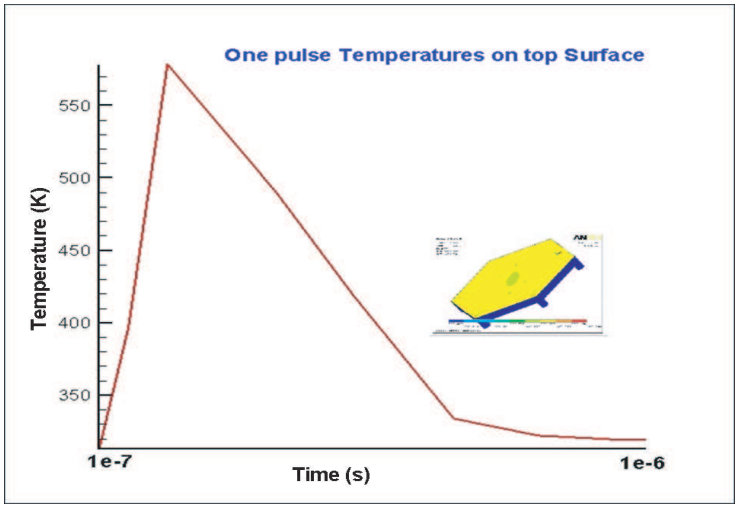

Figure 6.11: Thermal Response for 1 Pulse at Surface

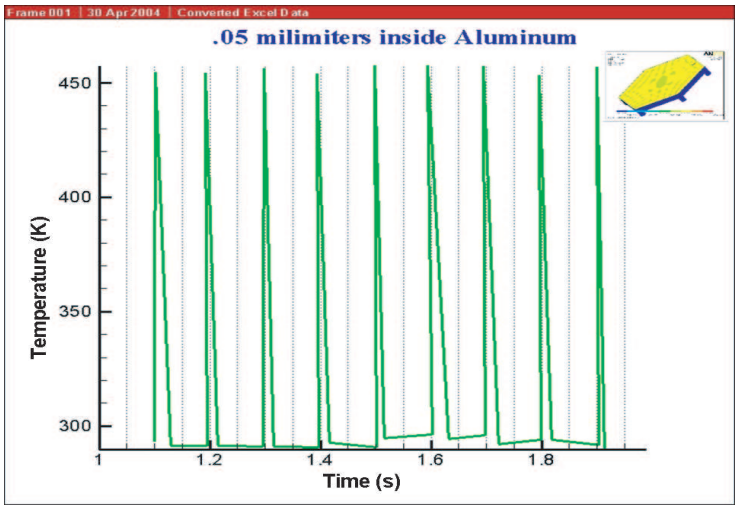

Figure 6.12: Thermal Response for 9 Pulses at 0.05 mm

Moving deeper into the material it is easy to see that the pulse has a milder

effect. Plots of one pulse at 0.5 mm and 9 pulses at the back surface are shown below. A decrease in temperature on the back surface is observed. This is due

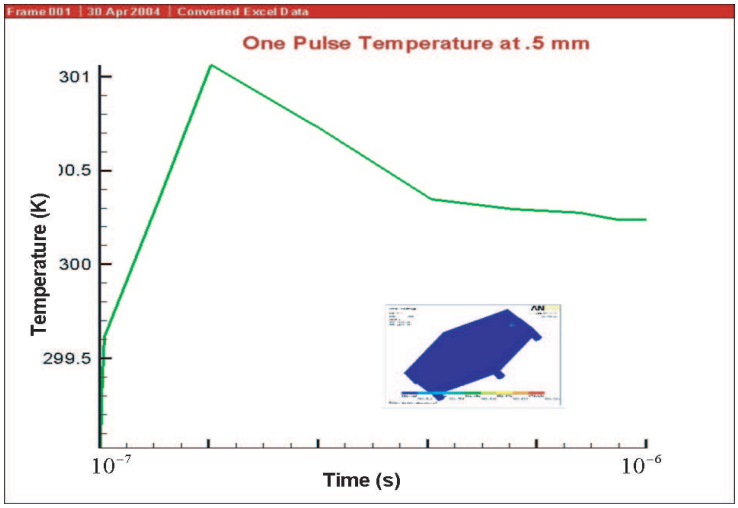

Figure 6.13: Thermal Response for 1 Pulse at .5 mm

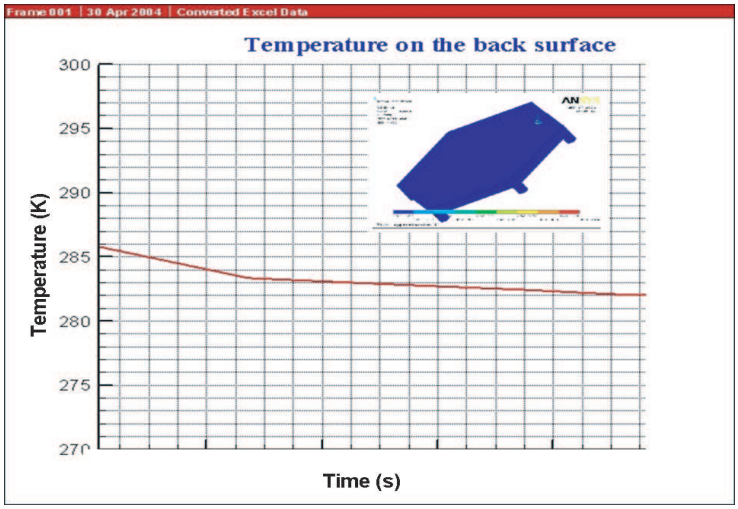

Figure 6.14: Thermal Response for 9 Pulses at the Back Surface

to the fact that this surface experiences more cooling form the convective load while it sees less on the actual thermal pulse. With the thermal response well

defined the question of induced stresses rises. Just as in the steady state analysis, the temperature distribution was exported to a different model for the transient mechanical analysis. In this case the model was simplified to a triangular section of the mirror. Symmetrical boundary conditions were applied and the stress response was recorded. The figures shows the stress increase in the section once

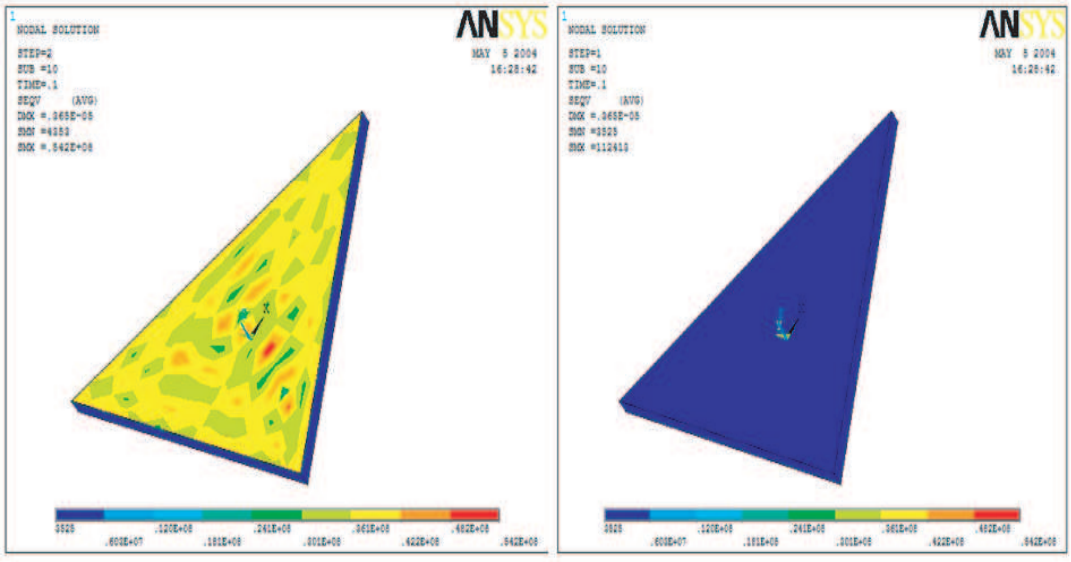

Figure 6.15: Stress Response Due to One Pulse

the laser pulse hits the surface and the final state at the end of the dissipation period, before the next pulse hits. It is evident that the average maximum surface stress experienced is around 36 MPa and the stress at the end of the dissipation period is around 30 KPa. Just from the plots above, it can be concluded that the maximum stress is not a threat to the structure since the yield stress of Aluminum 6061 is 125 MPa. Using the information provided by the results of the transient mechanical response an oscillatory behavior can be plotted. Figure 6.16 shows the cyclic behavior of the Aluminum mirror. With the maximum stress at 36 Mpa and minimum stress at 30 KPa, the mirror oscillates about the

18.015 MPa line. The information provided in the above graph was very useful

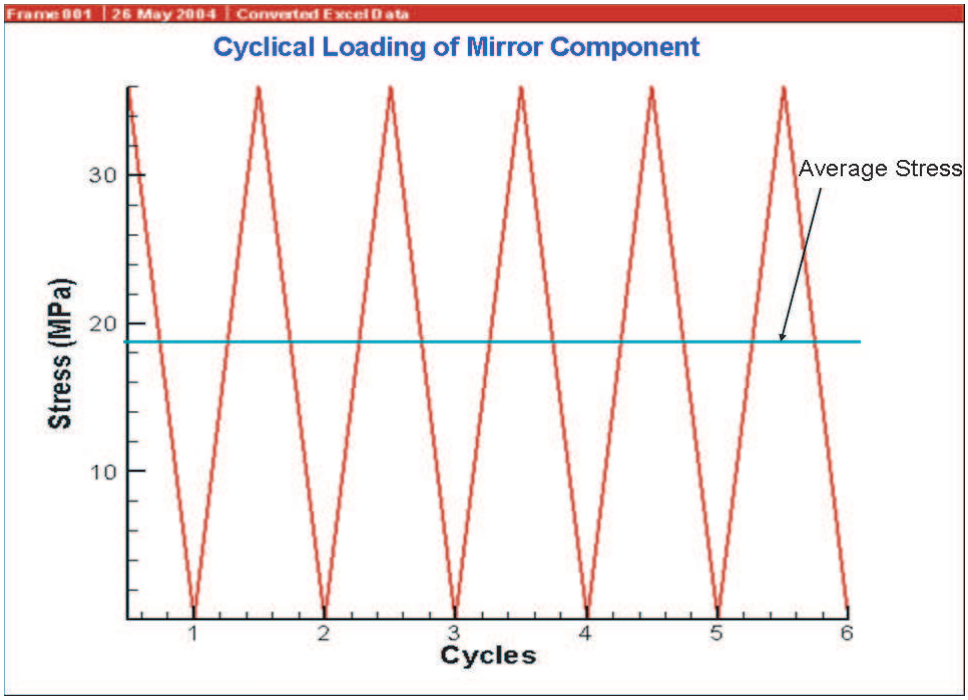

Figure 6.16: Cyclical Loading of UCLA Design

when implementing it to the general fatigue response of Aluminum 6061. In the next section the average load applied will be used and the life of the mirror will be investigated.

6.5 Fatigue Analysis of Alminum Mirrors

In order to consider the S-N curve for the Aluminum Alloy an alternating stress value had to be obtained. Using basic fatigue theory and information form the previous section it was found that σ_a= 18.015 MPa. This load will be mapped out on the S-N curve to find the maximum number of cycles the mirror would be able to withstand. Figure 6.17 shows different S-N curves for Aluminum alloys[**?**].

As it can be observed, the stress level imposed on the mirror surface by the

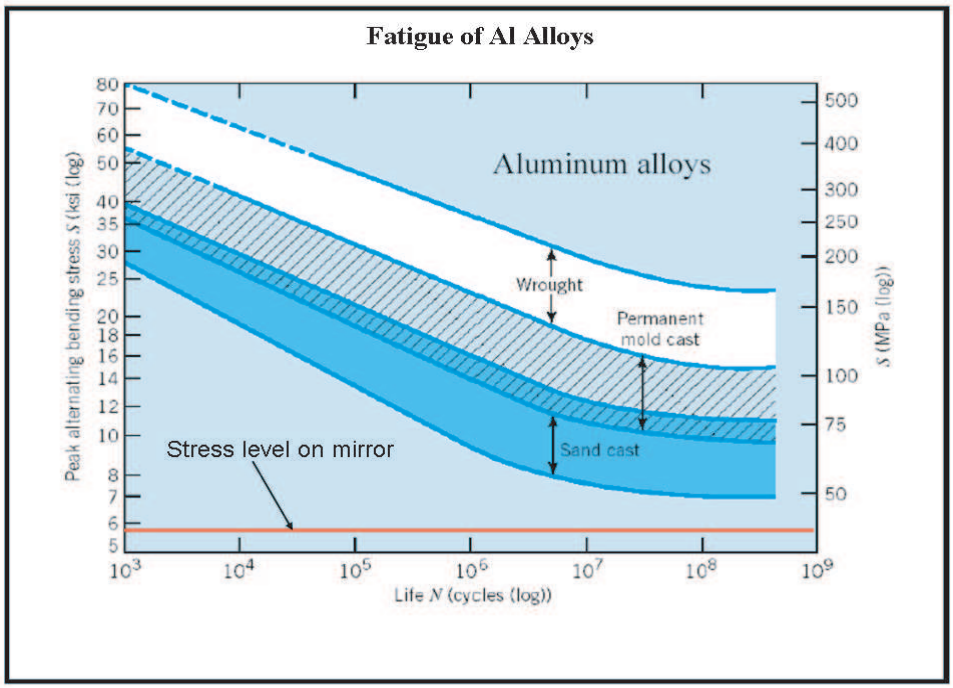

Figure 6.17: S-N Curve for Aluminum Alloys

thermal loading is very low even in comparison to the weakest kind of Aluminum Alloy. In reality, the mirror material would probably be in between the wrought and mold cases, leading to the conclusion that the mirror can almost sustain an infinite number of cycles. However, it is important to note that Aluminum and almost all nonferrous alloys do not have a "Fatigue Limit"-maximum stress level at which failure will not occur regardless of the number of cycles. This means that over an extremely long lifetime the material will finally fail. In the case of the UCLA Grazing Mirror we can assume that lifetime to be close to infinity since the applied load is small.

CHAPTER 7

Conclusions

The UCLA Final Optics solution has been shown to be a satisfactory and functional choice for the Inertial Confinement Fusion Process. Its characteristics make it a more convenient and economics focusing component than the KDP crystals discussed in Section 3.3(Figure 3.6). As mentioned before, the goal of this design work was to offer a plausible solution for the Inertial Confinement Fusion process that would be able to endure log term industrial use. Mainly for this purpose the choice was made to go from crystal type materials to metals. The UCLA Grazing Mirror design started from the basic idea of off-axis parabolic mirrors and was brought all the way to a complete 3D design. In order to complete this task the Solidworks CAD package was employed. All systems involved were created separately and then brought together to form the final mirror assembly. In regards to the performance of the design a few parameters were set in reference to what the mirror assembly should have to do as a Final Optics choice. Although there are many requirements for all systems involved some prevail for the overall design:

- Correctly reflect and focus the laser beam onto the target.
- Be able to withstand the temperature gradient caused by the laser pulses.
- Have a structurally sound design that can handle the mechanical stresses cause by the laser pulses.

- Have a deformable mirror configuration that is able to focus on the target within 5 percent error.
- Demonstrate a long functioning life under cyclical loading to ensure the possibility of industrial applications.

As demonstrated in the presented work, all requirements have been satisfied. First, the mathematical surface was designed for the mirror. Next, materials and dimensions have been assigned. Loads and constraints were applied using ANSYS and the results were then analyzed. As shown in Chapter 6 the standard error for the reflective surface was 5.5 percent which satisfies the focusing requirements. Again, the surface equation decided upon for this design was:

$$(Y - Y_0)^2 + (Z - Z_0)^2 = 2 * X \tag{7.1}$$

After the optical surface was constructed and analyzed, the thermo-mechanical performance was investigated. A cooling system was designed to ensure the functionality of the overall mirror system. After investigating different designs for cooling, using the COSMOS software package, a decision was made for a simple but effective piping system. After the implementation of cooling into the mirror assembly, a sequence of different analysis types was performed:

- Steady State Analysis for thermal response of surface: ΔT=2^o C.
- Steady State Analysis for the structural stresses due to the thermal gradient: σ=25 KPa.
- Transient Analysis for instantaneous thermal response of surface: ΔT=300^o C.
- Transient Analysis for the structural stresses due to the instantaneous thermal gradient: σ=36 MPa.

The thermal distribution plots and graphs shown in Chapter 6 demonstrate that the thermal requirements were also satisfied for the UCLA Grazing Mirror Design. The stress response is in conformity also, just as previously demonstrated in the same chapter. After obtaining the mechanical response, a fatigue performance estimation was shown. The alternating stress calculated was σ_a= 18.015 MPa. From the S-N curves for Aluminum it was easy to notice that the loading is very low and will potentially never cause any damage. The results of the fatigue analysis demonstrated that the UCLA design is a competitive candidate for a long term assignment as the Final Optics Segment for the Inertial Confinement Fusion Process. With the completion of the thermo-mechanical analysis of the 3D model for the model some important conclusions can be drawn. First, the UCLA Grazing Mirror Design satisfies all requirements for incorporation in the fusion process. Secondly, it shows definite advantages over the KDP crystal prisms by its longer lifetime and lower manufacturing cost. Thirdly, not only is it a completely designed 3D structure but it is also analyzed both analytically and by FEM software to ensure its future performance. Although most of the issues about the Final Optics Segment have been addressed in this thesis, there still are some areas that can be researched to further improve the UCLA design. Some of these areas can be identified as the following:

- Research of more material choices for the mirror surface, such as exotic composites with imbedded micro-actuators for better surface control.
- Additional transient analysis investigating the elasto-plastic area of the mirror mechanics for a more complete stress response.
- Further investigation in the arrangement of the mirrors around the target to find the most efficient solution.

- Development of a hydraulic support system that render the mirror mobile into almost any direction.

In conclusion, the thesis presented here offers a completely developed design for the Final Optics option with performances shown by FEM analysis and verified through analytical methods.

APPENDIX A

Sample Ansys Input Files

This section provides a few sample files that were used to simulate portions of the ANSYS analysis.

Transient Thermal Code.

The ANSYS code below shows a transient temp. input file.

```
/BATCH /COM,ANSYS RELEASE  5.7    UP20001208       16:46:26
08/27/2003 /input,menust,tmp     ,'',,,,,,,,,,,,,,,1 /GRA,POWER
/GST,ON /PLO,INFO,3 /COL,PBAK,ON,1,BLUE
/INPUT,'file827_2','txt','D:\shared\WORK\3-D Transient\','', 0
/COM,ANSYS RELEASE  5.7    UP20001208       16:47:45    08/27/2003
FINISH /SOLU FINISH /CLEAR,NOSTART /COM,ANSYS RELEASE  5.7
UP20001208       16:53:34    08/27/2003 !* RESUME /COM,ANSYS
RELEASE  5.7    UP20001208       16:53:42    08/27/2003 /SOLU !*
LSCLEAR,ALL FINISH /PREP7 FLST,2,2,6,ORDE,2 FITEM,2,1 FITEM,2,3
VCLEAR,P51X /REPLO /FOC, 1 ,0.300000,,,1 /REP,FAST FINISH !
/EXIT,NOSAV /BATCH /COM,ANSYS RELEASE  5.7    UP20001208 16:55:43
08/27/2003 /input,menust,tmp     ,'',,,,,,,,,,,,,,,1 /GRA,POWER
/GST,ON /PLO,INFO,3 /COL,PBAK,ON,1,BLUE /REPLOT,RESIZE !* /NOPR
```

```
/PMETH,OFF,0 KEYW,PR_SET,1 KEYW,PR_STRUC,1 KEYW,PR_THERM,1
KEYW,PR_FLUID,0 KEYW,PR_ELMAG,0 KEYW,MAGNOD,0 KEYW,MAGEDG,0
KEYW,MAGHFE,0 KEYW,MAGELC,0 KEYW,PR_MULTI,1 KEYW,PR_CFD,0 /GO !*
/COM, /COM,Preferences for GUI filtering have been set to display:
/COM,  Structural /COM,  Thermal !* /PREP7
MPREAD,'matprop','txt','..\Documents and
Settings\razvan1\Desktop\' !* ET,1,SOLID87 !* DOF,UX,UY,UZ
~PARAIN,aluminum8_27,x_t,'D:\shared\WORK\parasolid
folder\',SOLIDS,0,0 SMRT,6 SMRT,4 MSHAPE,1,3D MSHKEY,0 !*
CM,_Y,VOLU VSEL, , , ,       1 CM,_Y1,VOLU CHKMSH,'VOLU'
CMSEL,S,_Y !* VMESH,_Y1 !* CMDELE,_Y CMDELE,_Y1 CMDELE,_Y2 !*
CM,_Y,VOLU VSEL, , , ,       1 CM,_Y1,VOLU CMSEL,S,_Y !*
CMSEL,S,_Y1 VATT,       1, ,   1,       0 CMSEL,S,_Y CMDELE,_Y
CMDELE,_Y1 !* CM,_Y,VOLU VSEL, , , ,       1 CM,_Y1,VOLU
CMSEL,S,_Y !* CMSEL,S,_Y1 VATT,       1, ,   1,       0 CMSEL,S,_Y
CMDELE,_Y CMDELE,_Y1 !* FINISH /SOLU !* ANTYPE,4 !* TRNOPT,FULL
LUMPM,0 !* tunif,290 /units,mks

!!!!!!!!!!LOAD STEP 1 !* TIME,0.1 AUTOTS,-1 NSUBST,20,100,10,1
KBC,1 !* TSRES,ERASE FLST,2,3,3,ORDE,3 FITEM,2,2 FITEM,2,4
FITEM,2,6 !* /GO DK,P51X, ,0, ,0,UX, , , , , , FLST,2,1,5,ORDE,1
FITEM,2,7 /GO !* SFA,P51X,1,CONV,2000,288 LSWRITE,1,


!!!!!!!!!!LOAD STEP 2 !* TIME,0.100000002 AUTOTS,-1
NSUBST,10,100,10,1 KBC,0 !* TSRES,ERASE /USER, 1 /VIEW, 1,
0.585582091249    ,  0.146708333489    , -0.797226617276 /ANG,  1,
```

```
70.1787519744 /REPLO FLST,2,1,5,ORDE,1 FITEM,2,8 /GO !*
SFA,P51X,1,HFLUX,2e8 LSWRITE,2,


!!!!!!!!!!!LOAD STEP 3 !* TIME,0.2 AUTOTS,-1 NSUBST,20,100,10,1
KBC,1 !* TSRES,ERASE FLST,2,1,5,ORDE,1 FITEM,2,8
SFADELE,P51X,1,HFLUX LSWRITE,3,

!!!!!!!!!!!LOAD STEP 4

!* TIME,0.200000002 AUTOTS,-1 NSUBST,10,100,10,1 KBC,0 !*
TSRES,ERASE FLST,2,1,5,ORDE,1 FITEM,2,8 /GO !*
SFA,P51X,1,HFLUX,2e8 LSWRITE,4,


!!!!!!!!!!LOAD STEP 5 !* TIME,0.3 AUTOTS,-1 NSUBST,20,100,10,1
KBC,1 !* TSRES,ERASE FLST,2,1,5,ORDE,1 FITEM,2,8
SFADELE,P51X,1,HFLUX LSWRITE,5,

!!!!!!!!!!LOAD STEP 6

!* TIME,0.300000002 AUTOTS,-1 NSUBST,10,100,10,1 KBC,0 !*
TSRES,ERASE FLST,2,1,5,ORDE,1 FITEM,2,8 /GO !*
SFA,P51X,1,HFLUX,2e8 LSWRITE,6,


!!!!!!!!!!LOAD STEP 7 !* TIME,0.4 AUTOTS,-1 NSUBST,20,100,10,1
```

```
KBC,1 !* TSRES,ERASE FLST,2,1,5,ORDE,1 FITEM,2,8
SFADELE,P51X,1,HFLUX LSWRITE,7,


!!!!!!!!!!LOAD STEP 8 !*

TIME,0.400000002 AUTOTS,-1 NSUBST,10,100,10,1 KBC,0 !* TSRES,ERASE
FLST,2,1,5,ORDE,1 FITEM,2,8 /GO !* SFA,P51X,1,HFLUX,2e8 LSWRITE,8,


!!!!!!!!!!LOAD STEP 9 !* TIME,0.5 AUTOTS,-1 NSUBST,20,100,10,1
KBC,1 !* TSRES,ERASE FLST,2,1,5,ORDE,1 FITEM,2,8
SFADELE,P51X,1,HFLUX LSWRITE,9,


!NOW SOLVE THE SYSTEM

LSSOLVE,1,9,1,



!PLOT THE CENTER POINT FINISH /post26 ntrack1 =node(0.0,0.0,0.0)
nsol,2,ntrack1,temp,,W_sruf plvar,2
```

This section shows a sample loading file used to control the surface.

```
PRINT FZ   SUMMED NODAL LOADS

 ***** POST1 SUMMED TOTAL NODAL LOADS LISTING *****

 LOAD STEP=     1  SUBSTEP=     1
  TIME=    1.0000      LOAD CASE=   0

 THE FOLLOWING X,Y,Z SOLUTIONS ARE IN GLOBAL COORDINATES

   NODE      FZ
     17   1.2783
     20   1.1422
     22   1.0554
     24   1.0748
     26   1.0919
     28   1.3574
     81 -0.52602E-08
   7175 -0.80305E-08
   7200 -0.12215E-07
   7298 -0.44906E-08
   7346  -2.0000
   7366  -1.0000
   7712  0.35036E-08
```

```
 7730  -1.0000
10133  -3.0000
10477 -0.39691E-08

 TOTAL VALUES
 VALUE   0.45172E-08
```

The following sample file shows a transient stress analysis.

```
/COM,  Thermal !* /PREP7 !* ET,1,SOLID90 !*
MPREAD,'AL_mat_prop','txt','.\My Documents\transfer\WORK\3-D
Transient\' RPR4,3,0,0,0.05,0,3e-3 /USER,  1 /VIEW,  1,
0.540688514125    , -0.657231837070    ,  0.525073559642 /ANG,
1,  -30.1299484626 /REPLO /VIEW,  1, -0.729737805646    ,
-0.231170800725    ,  0.643461572982 /ANG,   1,   50.6247146363
/REPLO /VIEW,  1,  0.581939508645    , -0.619655247879    ,
0.526662873244 /ANG,   1,   5.56609858569 /REPLO /VIEW,  1,
-0.860394670377    ,  0.134196493489    ,  0.491642463912 /ANG,
1,   70.7261864233 /REPLO /VIEW,  1, -0.682255083803    ,
0.289785425794    ,  0.671232007298 /ANG,   1,   138.269347660
/REPLO /VIEW,  1, -0.600369886785    ,  0.342993775472    ,
0.722434266234 /ANG,   1,   138.162163258 /REPLO /VIEW,  1,
-0.161285313239    , -0.835157642450    , -0.525831493913 /ANG,
1,  -140.644347668 /REPLO /VIEW,  1, -0.489455579968    ,
-0.543577697055    ,  0.681877204856 /ANG,   1,   82.2236699550
/REPLO FLST,5,9,4,ORDE,2 FITEM,5,1 FITEM,5,-9 CM,_Y,LINE LSEL, , ,
```

```
,P51X CM,_Y1,LINE CMSEL,,_Y !* LESIZE,_Y1, , ,16, , , , ,1 !*
CM,_Y,VOLU VSEL, , , ,       1 CM,_Y1,VOLU CHKMSH,'VOLU'
CMSEL,S,_Y !* VSWEEP,_Y1 !* CMDELE,_Y CMDELE,_Y1 CMDELE,_Y2 !*
FINISH /SOL !* ANTYPE,4 !* TRNOPT,FULL LUMPM,0 !* SAVE /units,mks
tunif,300 /VIEW,  1, -0.873489998119E-01, -0.877677258247    ,
-0.471224768649 /ANG,   1,  -148.817064408 /REPLO
FLST,2,1,5,ORDE,1 FITEM,2,2 /GO ! write the first load step
SFA,P51X,1,CONV,2000,295 /VIEW,  1, -0.208221583164    ,
-0.923105661819    ,  0.323295081037 /ANG,   1,   80.4260838379
/REPLO /VIEW,  1, -0.307966273085    , -0.763526029227    ,
0.567613228647 /ANG,   1,   76.7032300172 /REPLO !* TIME,0.1
AUTOTS,-1 NSUBST,10,100,2,1 KBC,1 !* TSRES,ERASE LSWRITE,1,



!write the 1st pulse



FLST,2,1,5,ORDE,1 FITEM,2,1 /GO !* SFA,P51X,1,HFLUX,3e12 !*
TIME,0.100000003 AUTOTS,-1 NSUBST,10,100,2,1 KBC,1 !* TSRES,ERASE
LSWRITE,2,

!write the third load step


FLST,2,1,5,ORDE,1 FITEM,2,1 SFADELE,P51X,1,HFLUX !* TIME,0.2
```

```
AUTOTS,-1 NSUBST,10,100,2,1 KBC,1 !* TSRES,ERASE LSWRITE,3,


!write the 2nd pulse


FLST,2,1,5,ORDE,1 FITEM,2,1 /GO !* SFA,P51X,1,HFLUX,3e12 !*
TIME,0.200000003 AUTOTS,-1 NSUBST,10,100,2,1 KBC,1 !* TSRES,ERASE
LSWRITE,4,


!write the 5th load step


FLST,2,1,5,ORDE,1 FITEM,2,1 SFADELE,P51X,1,HFLUX !* TIME,0.3
AUTOTS,-1 NSUBST,10,100,2,1 KBC,1 !* TSRES,ERASE LSWRITE,5,


!write the 3rd pulse

FLST,2,1,5,ORDE,1 FITEM,2,1 /GO !* SFA,P51X,1,HFLUX,3e12 !*
TIME,0.300000003 AUTOTS,-1 NSUBST,10,100,2,1 KBC,1 !* TSRES,ERASE
LSWRITE,6,

! write the 7th load step
```

```
FLST,2,1,5,ORDE,1 FITEM,2,1 SFADELE,P51X,1,HFLUX !* TIME,0.4
AUTOTS,-1 NSUBST,10,100,2,1 KBC,1 !* TSRES,ERASE LSWRITE,7,


SAVE

LSSOLVE,1,7,1,




FINISH /POST26 FINISH /POST1 INRES,BASIC FILE,'file','rth','.'
FINISH /POST26 FILE,'file','rth','.' /UI,COLL,1 NUMVAR,200
SOLU,191,NCMIT STORE,MERGE FILLDATA,191,,,,1,1 REALVAR,191,191 !*
NSOL,2,763,TEMP,, TEMP_2 STORE,MERGE XVAR,1 PLVAR,2, EPLOT !*
NSOL,3,3144,TEMP,, TEMP_3 STORE,MERGE !* NSOL,4,736,TEMP,, TEMP_4
STORE,MERGE !* NSOL,5,808,TEMP,, TEMP_5 STORE,MERGE XVAR,1
PLVAR,4,

!face plot ntrack1 =node(0.0,0.0,0.0) nsol,5,ntrack1,temp,,front
face store, merge plvar,5
```

```
!face plot ntrack2 =node(0.0,0.0,0.0000001)
nsol,6,ntrack1,temp,,front face store, merge plvar,6




!face plot ntrack3 =node(0.0,0.0,0.0004)
nsol,7,ntrack1,temp,,front face store, merge plvar,7


save

/POST26 NUMVAR,200 FILLDATA,191,,,,1,1 REALVAR,191,191 !*
NSOL,8,761,TEMP,, TEMP_8 STORE,MERGE XVAR,1 PLVAR,8, EPLOT
/ZOOM,1,SCRN,0.629027,0.123632,0.688246,0.095771 !*
NSOL,9,3008,TEMP,, TEMP_9 STORE,MERGE !* NSOL,10,2824,TEMP,,
TEMP_10 STORE,MERGE !* NSOL,11,2615,TEMP,, TEMP_11 STORE,MERGE
XVAR,1 PLVAR,10,


SAVE
```

APPENDIX B

Sample Ansys Output Codes

The following output file presents the displacements of the nodes for the mirror unit segment after the application of actuator loads.

```
 PRINT U    NODAL SOLUTION PER NODE

  ***** POST1 NODAL DEGREE OF FREEDOM LISTING *****

 LOAD STEP=     1  SUBSTEP=     1
  TIME=    1.0000      LOAD CASE=   0

 THE FOLLOWING DEGREE OF FREEDOM RESULTS ARE IN GLOBAL COORDINATES

   NODE      UZ
      1  0.11543E-03
      2  0.12218E-03
      3  0.11495E-03
      4  0.12171E-03
      5  0.84965E-04
      6  0.91714E-04
      7  0.84749E-04
```

```
 8  0.91501E-04
 9  0.88844E-04
10  0.95602E-04
11  0.92624E-04
12  0.99400E-04
13  0.84602E-04
14  0.91367E-04
15  0.80242E-04
16  0.87010E-04
17   0.0000
18  0.69914E-05
19 -0.65622E-05
20   0.0000
21 -0.65780E-05
22   0.0000
23 -0.65752E-05
24   0.0000
25 -0.65710E-05
26   0.0000
27 -0.65235E-05
28   0.0000
29  0.12219E-03
30  0.12215E-03
31  0.12209E-03
32  0.12200E-03
33  0.12191E-03
34  0.12182E-03
```

```
    35  0.12175E-03
    36  0.12169E-03
    37  0.12174E-03

***** POST1 NODAL DEGREE OF FREEDOM LISTING *****

LOAD STEP=     1  SUBSTEP=     1
 TIME=    1.0000      LOAD CASE=   0

THE FOLLOWING DEGREE OF FREEDOM RESULTS ARE IN GLOBAL COORDINATES

  NODE      UZ
    38  0.12180E-03
    39  0.12188E-03
    40  0.12196E-03
    41  0.12205E-03
    42  0.12213E-03
    43  0.92811E-04
    44  0.93651E-04
    45  0.94004E-04
    46  0.94051E-04
    47  0.93783E-04
    48  0.93230E-04
    49  0.92422E-04
    50  0.90418E-04
    51  0.89597E-04
    52  0.89254E-04
```

```
    53  0.89206E-04
    54  0.89468E-04
    55  0.90003E-04
    56  0.90798E-04
    57  0.95273E-04
    58  0.95409E-04
    59  0.95820E-04
    60  0.96440E-04
    61  0.97209E-04
    62  0.98019E-04
    63  0.98805E-04
    64  0.99741E-04
    65  0.99591E-04
    66  0.99164E-04
    67  0.98526E-04
    68  0.97750E-04
    69  0.96942E-04
    70  0.96178E-04
    71  0.90598E-04
    72  0.89523E-04
    73  0.88646E-04
    74  0.87840E-04

***** POST1 NODAL DEGREE OF FREEDOM LISTING *****

LOAD STEP=     1  SUBSTEP=     1
 TIME=    1.0000      LOAD CASE=   0
```

THE FOLLOWING DEGREE OF FREEDOM RESULTS ARE IN GLOBAL COORDINATES

NODE	UZ
75	0.87198E-04
76	0.86812E-04
77	0.86738E-04
78	0.87760E-04
79	0.88814E-04
80	0.89692E-04
81	0.90506E-04
82	0.91168E-04
83	0.91570E-04
84	0.91651E-04
85	-0.55492E-05
86	-0.45118E-05
87	-0.24434E-05
88	-0.38839E-06
89	0.16424E-05
90	0.36570E-05
91	0.56489E-05
92	0.75948E-05
93	0.94735E-05
94	0.11288E-04
95	0.13035E-04
96	0.14704E-04
97	0.16283E-04

```
    98  0.17767E-04
    99  0.19157E-04
   100  0.20445E-04




 ***** POST1 NODAL DEGREE OF FREEDOM LISTING *****

 LOAD STEP=     1  SUBSTEP=     1
  TIME=    1.0000      LOAD CASE=   0


MAXIMUM ABSOLUTE VALUES
NODE       7298
VALUE   0.12895E-03
```

APPENDIX C

Additional Materials on Designs and Properties of Aluminum

This section presents previous designs used for the UCLA grazing mirror and some Aluminum material properties.

C.1 Some Important Properties of Aluminum

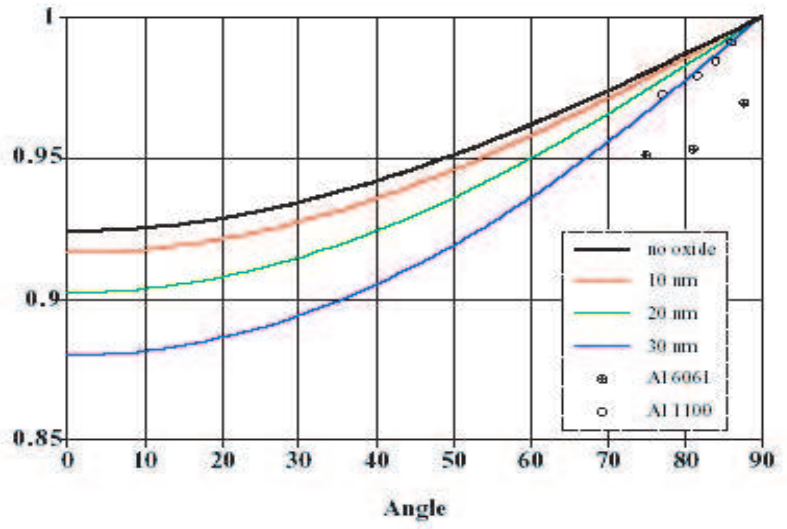

Figure C.1: Reflectivity vs. Grazing Angle

The following is an extensive list of properties which were also used:

Atomic Properties

Atomic number 13 Atomic radius - Goldschmidt (nm) 0.143

Atomic weight (amu) 26.98154

Crystal structure Face centred cubic
Electronic structure Ne 3s2
3p1 Ionization potential No. eV
1 5.99
2 18.8
3 28.4
4 120
5 154
6 190
Natural isotope distribution Mass No. %
27 100
Photo-electric work function (eV) 4.2 Thermal neutron absorption
cross-section (Barns) 0.232 Valences shown 3

Electrical Properties Temperature coefficient @0-100C (K-1)
0.0045 Electrical resistivity @20C (Ohmcm) 2.67
Superconductivity critical temperature (K) 1.175 Thermal emf
against Pt (cold 0C - hot 100C) (mV) +0.42

Mechanical Properties Material condition Soft Hard Polycrystalline Bulk modulus (GPa) 75.2 Hardness - Vickers 21 35-48 Poisson's ratio 0.345 Tensile modulus (GPa) 70.6 Tensile strength (MPa) 50-90 130-195 Yield strength (MPa) 10-35 110-170

Physical Properties Boiling point (C) 2467 Density @20C (g cm-3) 2.70 Melting point (C) 660.4

Thermal Properties Coefficient of thermal expansion @0-100C (x10-6 K-1) 23.5 Latent heat of evaporation (J g-1) 10800 Latent heat of fusion (J g-1) 388 Specific heat @25C (J K-1 kg-1) 900 Thermal conductivity @0-100C (W m-1 K-1) 237

Properties for Aluminum Honeycomb Property Value Cell Size mm 19 6.3 13 4.8 3.2 6.3 Compressive Strength MPa 0.7 2.1 2.9 3.5 3.7 4.6 Density g cm-3 0.029 0.054 0.062 0.07 0.072 0.083 Plate Shear Modulus - Longitudinal MPa 120 270 310 360 370 430 Plate Shear Modulus - Transverse MPa 70 170 200 225 230 270 Plate Shear Strength - Longitudinal MPa 0.6 1.5 1.8 2.2 2.3 2.9 Plate Shear Strength - Transverse MPa 0.45 1.0 1.2 1.4 1.5 1.8 Wall Thickness mm 0.064 0.038 0.102 0.038 0.025 0.064

C.2 Previous designs for the UCLA Grazing Mirror

This sections shows a series of figures containing earlier designs of the UCLA project.

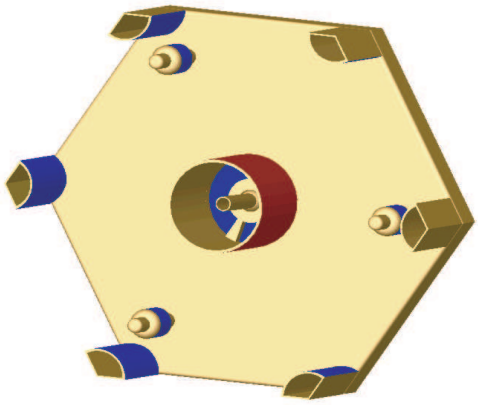

Figure C.2: 2002 Unit Mirror Design

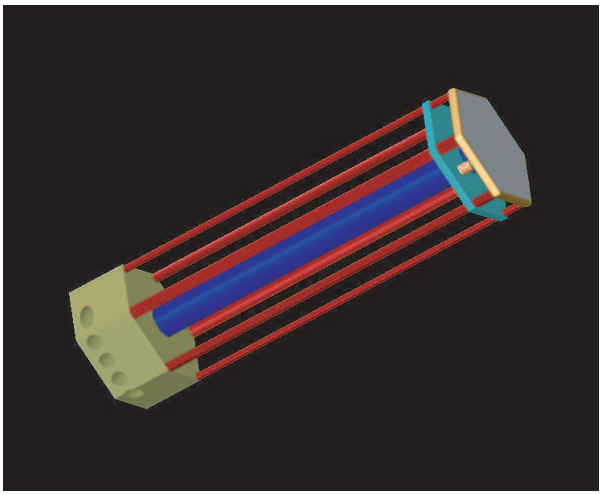

Figure C.3: 2002 Cooling Option

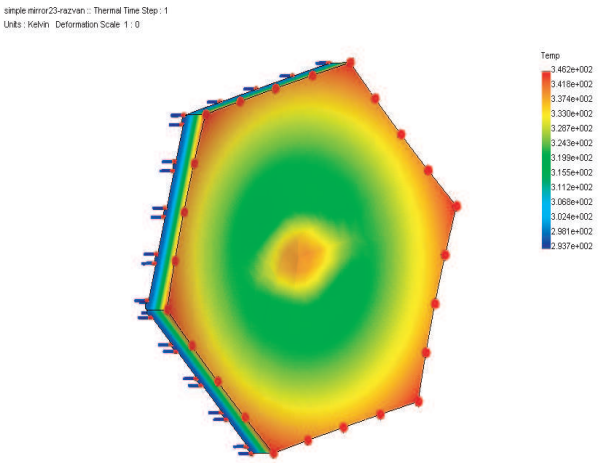

Figure C.4: 2002 COSMOS temp response

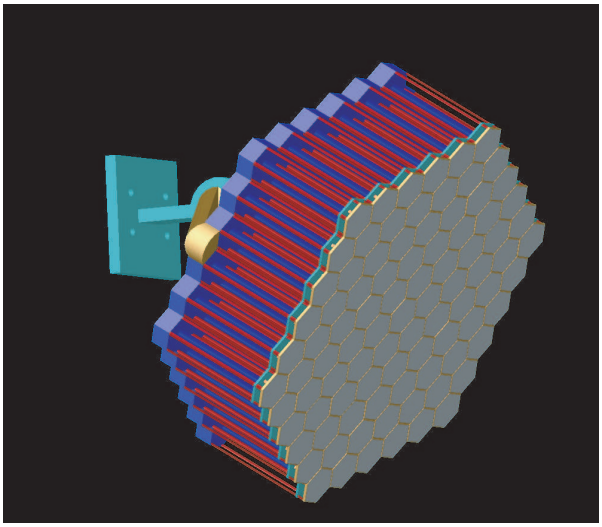

Figure C.5: 2002 Final Assembly

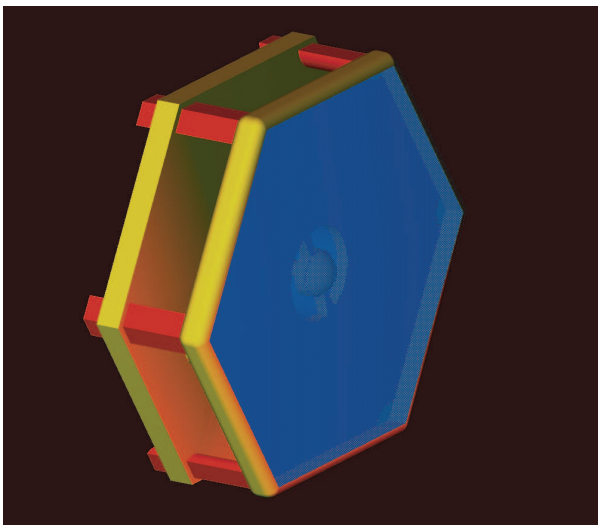

Figure C.6: 2003 Unit Mirror

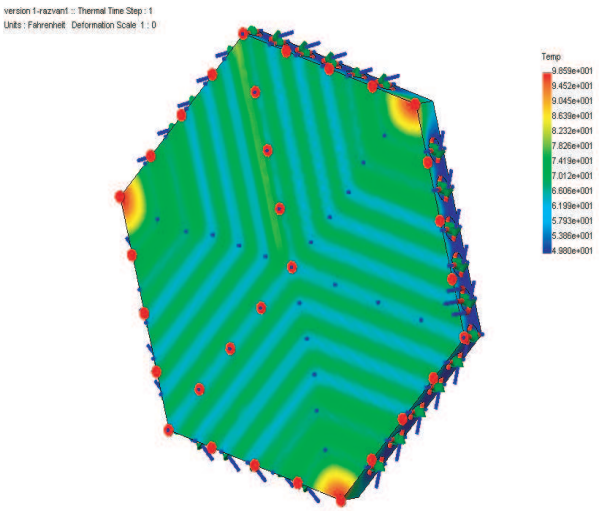

Figure C.7: 2003 Cooling Option

References

[1] General Atomics. Inertial confinement fusion. Web Site, 2004. .

[2] James P. Blanchard. Practical considerations for thermal stresses induced by surface heating. 2000.

[3] COSMOSWorks^{TM}. Cosmos s.s. tutorial. Web Site, 2004. .

[4] Douglas G. MacMartin Gary Chanan. Control and alignment of segmented-mirror telescopes: matrices, modes, and error propagation. *APPLIED OPTICS*, 43(6):2–6, February 2004. .

[5] ANSYS Inc. Ansys 7.1 documentation. 2003.

[6] Roy R. Craig Jr. *Mechanics of Materials*. Wiley, 2000.

[7] Lawrence Livermore National Laboratories. National ignition facility projects. Web Site, 2004. .

[8] MathWorld. Parabolic mirrors. Web Article, 2004. .

[9] Claire Max. Wavefront correction: Deformable mirrors. Presentation, April 2002. .

[10] A. F. Mills. *Basic Heat and Mass Transfer*. Prentice Hall, 1999.

[11] K Sequoia M.S Tillack, J.E Pulsifer. Uv laser induced damage to grazing incidence metal mirrors. *TuO8.2*, pages 1–4, 2001.

[12] Scot S. Olivier. Wavefront correction technologies. , 2004.

[13] David Roylance. Fatigue. *Department of Materials Science and Engineering*, ( ):4–8, 2001. .

[14] R. Makidon R. Winsor, A. Sivaramakrishnan. Finite element analysis of low cost membrane deformable mirrors for high order adaptive optics. *Space Telescope Science Institute*, ( ):1–7, 2004. .

[15] Mark S. Tillack. Final optic research on grazing incidence metal mirrors. , 2001.

[16] Andrei A. Tokovinin. Tutorial on adaptive optics at ctio. Web Article, 2004. .

[17] Michel Verhaegen. Control of a deformable mirror for adaptive optics focussing. *Delft Center for Control Systems*, ( ), 2004. .

[18] L. H. Van Vlack. *Elements of Materials Science and Engineering*. Prentice Hall, 1989.